Bacillus velezensis HBXN2020 alleviates *Salmonella* Typhimurium-induced colitis by improving intestinal barrier integrity and reducing inflammation

Linkang Wang,[1,2,3] Haiyan Wang,[1,2,3] Xinxin Li,[1,2,3] Mengyuan Zhu,[1,2,3] Dongyang Gao,[1,2,3] Dayue Hu,[1,2,3] Zhixuan Xiong,[1,2,3] Xiangmin Li[1,2,3]* and Ping Qian[1,2,3]*

[1]*National Key Laboratory of Agricultural Microbiology, Hubei Hongshan Laboratory, Huazhong Agricultural University, Wuhan, Hubei, 430070, People's Republic of China*.

[2]*College of Veterinary Medicine, Huazhong Agricultural University, Wuhan, Hubei, People's Republic of China*.

[3]*Key Laboratory of Preventive Veterinary Medicine in Hubei Province, the Cooperative Innovation Center for Sustainable Pig Production, Wuhan, Hubei, People's Republic of China*.

* Corresponding author: Ping Qian: Tel: 86-27-87282608; Fax: 86-27-87282608; E-mail: qianp@mail.hzau.edu.cn. Address: No. 1, Shizishan Street, Hongshan District, Wuhan City, Hubei Province, China.

* Co-corresponding author: Xiang-min Li: Tel: 86-27-87282608; Fax: 86-27-87282608; E-mail: lixiangmin@mail.hzau.edu.cn. Address: No. 1, Shizishan

Street, Hongshan District, Wuhan City, Hubei Province, China.

Abstract

Bacillus velezensis is a novel species of Bacillus that has been widely investigated because of its broad-spectrum antimicrobial activity. However, most studies on *Bacillus velezensis* have focused on biocontrol of plant diseases, with few reports on antagonizing *Salmonella* Typhimurium infections. In this study, *Bacillus velezensis* HBXN2020 was isolated from healthy black piglets and was found to exhibit broad-spectrum antibacterial activity and robust anti-stress capabilities. Importantly, *Bacillus velezensis* HBXN2020 did not cause any adverse side effects in mice when administered at various doses (1×10^7, 1×10^8, and 1×10^9 CFU) for 14 days. In a *Salmonella* Typhimurium ATCC14028-induced mice colitis model, either curative or prophylactic, supplementing *Bacillus velezensis* HBXN2020 spores significantly lowered the levels of *Salmonella* Typhimurium ATCC14028 in their feces, ileum, cecum, and colon, and the disease activity index (DAI). Importantly, supplementing *Bacillus velezensis* HBXN2020 spores significantly regulated cytokine levels (TNF-α, IL-1β, IL-6, and IL-10) and maintained the expression of tight junction proteins and mucin protein. More importantly, supplementing *Bacillus velezensis* HBXN2020 spores also significantly enhanced the homeostasis of colonic microbiota and the abundance of beneficial bacteria. Collectively, *Bacillus velezensis* HBXN2020

can alleviate bacterial colitis by enhancing intestinal homeostasis and gut barrier integrity and reducing inflammation.

Key words: *Bacillus velezensis*; antibacterial activity; *S.* Typhimurium-induced colitis; infections; gut health

Introduction

Salmonella Typhimurium (*S.* Typhimurium) is a major foodborne zoonotic pathogen that can cause diarrhea and colitis in humans and animals (1, 2). It has been reported that *Salmonella* infections often occur in both developing and developed countries, which poses a substantial risk to public health and causes huge economic loss (3, 4). At present, antibiotic therapies is one of the most effective strategies for *Salmonella* infections. However, numerous studies have reported that the prolonged use or misuse of antibiotics can lead to environmental pollution, an increase in multi-drug-resistant (MDR) bacteria, as well as gastrointestinal microbiota dysbiosis (5-7). Therefore, there is an emergent search for novel antimicrobial agents to combat *Salmonella* infections.

Recently, an increasing number of studies have shown that gut microbiota plays an important role in alleviating intestinal inflammation (8) and repairing the intestinal barrier (9, 10). The use of probiotics is a popular approach to modulate intestinal microbiota nowadays. Among all probiotics, Bacillus is one of the most popular probiotic species because of their ability to form

endospores that survive gastric transit, storage and delivery conditions (11). In addition, Bacillus species can also produce antimicrobial metabolites against enteric pathogens and provide extracellular enzymes, thereby reducing infection risk and improving nutrient utilization (12, 13).

Bacillus velezensis (*B. velezensis*), a newly discovered species of the *Bacillus* genus, can produce an abundance of secondary metabolites with broad-spectrum antibacterial activity (14). Previous studies have reported that *B. velezensis* exhibits varying degrees of probiotic effects on plants, livestock, poultry and fish. For instance, the combined use of *B. velezensis* SQR9 mutant and FZB42 improved root colonization and the production of secondary metabolites that are beneficial to cucumber (15). *B. velezensis* isolated from yaks was shown to enhance growth performance and ameliorate blood parameters related to inflammation and immunity in mice (16). The dietary *B. velezensis* supplementation can regulate the innate immune response in the intestine of crucian carp and reduce the degree of intestinal inflammation damage induce by *A. veronii* (17). However, most studies on *B. velezensis* were mainly biocontrol of plant fungal diseases, with few reports on the treatment or prevention of *S.* Typhimurium-induced colitis.

In this study, we have screened a strain of *B. velezensis* HBXN2020 with broad-spectrum antibacterial activity from a large number of *Bacillus* strains. We aimed to investigate the effectiveness of *B. velezensis* HBXN2020 in alleviating *S.* Typhimurium-induced mouse colitis and assessed the biological

safety of *B. velezensis* HBXN2020. Notably, *B. velezensis* HBXN2020 can alleviate symptoms and colon tissue damage in experimental colitis, as indicated by markers such as *S.* Typhimurium loads, TNF-α and ZO-1 levels. Moreover, *B. velezensis* HBXN2020 was also enhanced the homeostasis of colonic microbiota and the abundance of beneficial bacteria (*Lactobacillus* and *Akkermansia*). Therefore, this study provides support for the development of probiotic-based microbial products as an alternative prevention strategy for *Salmonella* infection.

Results

Genomic Characteristics

The Illumina Hiseq and PacBio platforms were used to perform whole genome sequencing of HBXN2020, yielding a total of 8,194,986 Illumina clean reads (1,237,442,886 bases) and 225,593 PacBio reads (1,807,288,759 bases). Following a quality assessment via k-mer and a GC-depth analysis, the whole genome was assembled *de novo* using Unicycler (Version 0.4.8). The results showed that HBXN2020 has a circular chromosome of 3,929,792 bp (Fig. 1A) with a GC content of 46.5%. The genome of HBXN2020 was predicted to contain 3,857 genes, including 3,744 protein-coding genes (CDS), 86 tRNA genes, and 27 rRNA genes (Table S1).

A phylogenetic tree based on genome-wide data from all 14 Bacillus strains demonstrated that the HBXN2020 belongs to the *B. velezensis* species (Fig.

111 1B). To further understand the classification status of HBXN2020, the online
112 tool JSpeciesWS was used to calculate the average nucleotide identity (ANI)
113 based on the BLAST (ANIb) method. As shown in Fig. 1C, HBXN2020 was
114 found to be a member of the *B. velezensis* species due to the high percentage
115 of ANIb (more than 97%).
116
117 **Growth curve of *B. velezensis* HBXN2020 and its *in vitro* resistance**
118 **against environmental assaults.**
119 The growth of *B. velezensis* HBXN2020 was assessed in flat-bottomed 100-
120 well microtiter plates by measuring the values of OD_{600} every hour using an
121 automatic growth curve analyzer. The OD_{600} value of *B. velezensis*
122 HBXN2020 showed slight fluctuations within the first 2 h, followed by a
123 logarithmic growth phase that reached a stable phase after 10 h (Fig. 2A).
124 Despite environmental restrictions such as limited space and nutrients, the
125 OD_{600} value of the bacteria was not significantly reduced even after 22 h,
126 indicating that the growth of *B. velezensis* HBXN2020 was relatively stable.
127 Next, we evaluated the effect of physical, chemical, and biological
128 sterilization conditions such as high temperature, strong acidity, and enzyme
129 preparation on the survival of *B. velezensis* HBXN2020. The survival rate of *B.*
130 *velezensis* HBXN2020 showed a decreasing trend with increasing
131 temperature. At 65°C, the survival rate of *B. velezensis* HBXN2020 was less
132 than 1%, while the spores of *B. velezensis* HBXN2020 exceeded 90% (Fig.

133 2B). The survival rate of *B. velezensis* HBXN2020 spores was also above 80%
134 even under high-temperature conditions (95°C). Similar results were observed
135 following exposure to a strong acid environment (pH 2.0) (Fig. 2C), whereby *B.*
136 *velezensis* HBXN2020 spores were found to effectively tolerate strong acidic
137 conditions and exhibited improved survival rate. Based on these results, we
138 hypothesized that *B. velezensis* HBXN2020 spores might also exhibit
139 improved survival in gastrointestinal tract environments. Therefore, we further
140 evaluated the survival rate of *B. velezensis* HBXN2020 in bile salt (0.3%, v/v),
141 simulated gastric fluid (pepsin 1 mg mL^{-1}, pH 1.2), and simulated intestinal
142 fluid (trypsin 1 mg mL^{-1}, pH 6.8). As shown in Fig. 2D-F, *B. velezensis*
143 HBXN2020 spores demonstrated significantly improved tolerance to these
144 simulated gastrointestinal tract environments.
145

146 **Antibiotic susceptibility of *B. velezensis* HBXN2020 and bacteriostasis**
147 **effect *in vitro*.**

148 To evaluate the drug resistance of *B. velezensis* HBXN2020, 19 commonly
149 used antibiotics in clinical practice were selected. The results indicated that
150 only polymyxin B had a relatively small inhibition zone diameter (less than 15
151 mm). Ampicillin, meropenem, minocycline, ofloxacin, and trimethoprim had
152 the strongest inhibition on *B. velezensis* HBXN2020, with an inhibition zone
153 diameter exceeding 30 mm (Fig. 3A). In addition, the experimental results
154 showed that *B. velezensis* HBXN2020 was extremely sensitive to β-lactams,

tetracyclines, and quinolone drugs. Then, we performed an inhibition test of *B. velezensis* HBXN2020 against seven common clinical pathogenic bacteria. The results showed that *B. velezensis* HBXN2020 had a similar inhibitory effect on standard and wild strains of *E. coli*, *Salmonella*, *S. aureus*, and *C. perfringens*, as well as wild strains of *S. suis*, *P. multocida*, and *A. pleuropneumoniae*. Except for the wild strains of *S. suis* and *A. pleuropneumoniae*, the diameter of the inhibition zone of other strains was above 15 mm (Fig. 3B, S3), while the size of the inhibition zone of *S. suis* and *A. pleuropneumoniae* was also more than 12 mm.

Biosafety evaluation of *B. velezensis* HBXN2020

To determine the safety of *B. velezensis* HBXN2020, we evaluated its biological safety in a mouse model. After gavage with *B. velezensis* HBXN2020 spores for two weeks, we observed no significant difference in the body weight of each group of mice (Fig. 4A). The gene expression levels of TNF-α, IL-1β, IL-6, and IL-10 of colon from all groups of mice exhibited no remarkable changes (Fig. 4B). However, in the colon, mRNA levels of the barrier proteins ZO-1 and occludin were trending towards an increase compared with the control group (Fig. 4C). Additionally, blood routine tests and serum biochemistry tests were performed for mice in the control group and H-HBXN2020 group on the 14th day after oral administration of *B. velezensis* HBXN2020 spores multiple times. As shown in Fig. 4D and S1, the

177 blood parameters of mice after *B. velezensis* HBXN2020 treatment, including
178 red blood cells (RBC), mean corpuscular volume (MCV), mean corpuscular
179 hemoglobin (MCH), hemoglobin (HGB), white blood cells (WBC), platelets
180 (PLT), hematocrit (HCT), and mean corpuscular hemoglobin concentration
181 (MCHC), were consistent with those of healthy mice. The serum biochemical
182 parameters, including alanine aminotransferase (ALT), aspartate
183 aminotransferase (AST), albumin (ALB), total bilirubin (TBIL), serum
184 creatinine (CREA), and blood urea nitrogen (BUN), were also within normal
185 limits (Fig. 4E). The corresponding histological analysis of colon tissue from
186 mice receiving low, medium, and high doses of *B. velezensis* HBXN2020
187 spores (L-HBXN2020, M-HBXN2020, and H-HBXN2020 groups, respectively)
188 is presented in Fig. 4F. The colon tissue sections of mice in the test groups
189 showed no significant differences compared to the control group. Additionally,
190 there were no observable differences in the major organ tissues (heart, liver,
191 spleen, lung, and kidney) of mice treated with the high dose of *B. velezensis*
192 HBXN2020 spores compared to healthy mice (Fig. S2). Collectively, these
193 experimental results indicate that *B. velezensis* HBXN2020 is safe for use and
194 does not cause any adverse side effects in mice.
195
196 **Oral administration of *B. velezensis* HBXN2020 spores alleviated *S.***
197 **Typhimurium-induced colitis.**
198 To investigate whether *B. velezensis* HBXN2020 could inhibit *S.*

199 Typhimurium ATCC14028 (STm), solid and liquid co-culture tests were
200 conducted, and the results showed that *B. velezensis* HBXN2020 inhibited the
201 growth of STm in a dose-dependent manner (Fig. 5A, S4A-B, S4D). Next, the
202 therapeutic potential of *B. velezensis* HBXN2020 was evaluated in an STm-
203 induced mouse colitis model. At days 1, 3, and 5 after STm infection, mice in
204 the STm + HBXN2020 group were orally administered *B. velezensis*
205 HBXN2020 spores by gavage (Fig. 5B), while the control group and STm +
206 PBS group were treated with sterile PBS. Also, the number of excreted STm
207 in feces was counted daily at the designated time points. As shown in Fig. 5C,
208 there was a significant and continuous reduction in the number of STm in
209 feces following treatment with *B. velezensis* HBXN2020 spores, while the
210 number of *B. velezensis* HBXN2020 viable bacteria in feces is also gradually
211 decreasing (Fig. S5A). The number of STm in mouse feces was reduced by
212 10 to 50 times compared to the STm + PBS group from day 2 to 7 post-
213 treatment. *B. velezensis* HBXN2020 spore treatment also resulted in a 5 to
214 10-fold reduction in the number of STm in the ileum, cecum, and colon,
215 respectively (Fig. 5D-E, S5B). The increased inhibition of STm after *B.*
216 *velezensis* HBXN2020 spore treatment also resulted in less weight loss and a
217 marked reduction ($P < 0.001$) in DAI scores in STm + HBXN2020 group mice
218 (Fig. 5F-G). In addition, we also measured the colon length of the mice and
219 found that the STm + PBS group had a significantly shorter colon length ($P <$
220 0.001) than the control group. However, compared to the STm + PBS group,

221 the STm + HBXN2020 group exhibited a longer colon ($P < 0.05$) (Fig. 5H-I).

222 To further assess the impact of *B. velezensis* HBXN2020 on the intestinal
223 tract, we histologically analyzed their colonic tissues. The results showed that
224 mice treated with *B. velezensis* HBXN2020 spores exhibited a lower histology
225 score (total scoring) ($P < 0.05$) (Fig. S5C) than mice not treated with the
226 spores and were similar to that of healthy mice (control group). The colon
227 tissue of mice not treated with *B. velezensis* HBXN2020 spores displayed
228 higher histological scores, with significant crypt deformation, severe mucosal
229 damage, and obvious inflammatory cell infiltration. These findings suggest
230 that *B. velezensis* HBXN2020 can alleviate colon tissue damage. Moreover,
231 we measured the mRNA levels of inflammatory cytokines, including tumor
232 necrosis factor-α (TNF- α), interleukin-1 β (IL-1 β), interleukin-6 (IL-6), and
233 interleukin-10 (IL-10) in colon tissue using RT-qPCR analysis. As shown in
234 Fig. 6B-D, the mRNA levels of TNF-α ($P < 0.01$), IL-1β ($P < 0.05$), and IL-6 (P
235 < 0.05) in the colon tissue of STm-infected mice were significantly upregulated,
236 indicating the successful establishment of the STm-induced colitis model. As
237 expected, treatment with *B. velezensis* HBXN2020 spores led to a significant
238 reduction in the mRNA levels of these pro-inflammatory cytokines, while the
239 mRNA levels of the anti-inflammatory cytokine IL-10 were significantly
240 increased ($P < 0.01$) (Fig. 6E), suggesting that *B. velezensis* HBXN2020
241 spores can alleviate the inflammatory reaction of the colon. Moreover, the
242 mRNA expression levels of colonic epithelial barrier proteins, including ZO-1,

243 ocludin, claudin, and Muc2, were also measured by RT-qPCR. Compared
244 with the PBS-treated group, the *B. velezensis* HBXN2020 spores treatment
245 group exhibited significantly upregulated mRNA expression levels of ZO-1 (P
246 < 0.05), occludin ($P < 0.05$), claudin ($P < 0.05$), and Muc2 ($P < 0.01$) in the
247 colon tissue (Fig. 6F-I), further demonstrating the ability of *B. velezensis*
248 HBXN2020 to reduce damage to the colon epithelial barrier.

249 Next, we further explored the effect of HBXN2020 spores on the intestinal
250 microbiota composition of STm-treated mice via 16S rRNA gene sequencing.
251 The alpha diversity of colonic microbiota was evaluated using Sobs, Chao1,
252 Shannon, and Simpson indices (OTU levels). Compared with the control and
253 HBXN2020 group, the Sobs, Chao1, and Shannon indices of the STm + PBS
254 group clearly decreased (Fig. 7A-C), while the Simpson index significantly
255 increased ($P < 0.05$, Fig. 7D). Principle component analysis (PCA) based on
256 Bray–Curtis distance showed that compared with the STm + PBS group, the
257 gut microbiota composition of the STm + HBXN2020 group and the control
258 group were more closer together ($R = 0.3988$, $P = 0.001$, Fig. 7E). We analyzed
259 the significance of differences among groups at different classification levels
260 (Fig. 7F-G), and the results revealed that the composition of the gut
261 microbiota changed markedly after STm-induced mice. At the phylum level,
262 the STm + PBS group increased the abundance of *Verrucomicrobiota* and
263 *Proteobacteria* and decreased the abundance of *Firmicutes*, *Patescibacteria*,
264 *Desulfobacterota*, and *Actinobacteriota* compared to the Control group (Fig.

7F). The HBXN2020 group increased the abundance of *Bacteroidota* and *Firmicutes* and decreased the abundance of *Verrucomicrobiota* compared with the Control group. On the contrary, the relative abundance of *Firmicutes*, *Patescibacteria*, *Desulfobacterota*, and *Actinobacteriota* in the STm + HBXN2020 group was significantly higher than that in the STm + PBS group. At the genus level, infection with *S.* Typhimurium ATCC14028 in the STm + PBS group dramatically reduced the relative abundance of *norank_f_Muribaculaceae* and *Lactobacillus* (Fig. 7H-I) and enhanced the abundance of *Bacteroides*, *Escherichia-Shigella*, *Salmonella*, *Alistipes*, and *Enterococcus* compared to the Control group (Fig. 7J-K, S6B). The HBXN2020 group increased the abundance of *norank_f_Muribaculaceae* and *Alloprevotella* compared to the Control group. In contrast, STm + HBXN2020 group significantly improved the relative abundance of *norank_f_Muribaculaceae* and *Lactobacillus* compared with the STm + PBS group ($P < 0.01$, $P < 0.001$, Fig. 7H-I). In addition, LEfSe analysis was also performed to identify specialized microbial communities between the STm + HBXN2020 group and the STm + PBS group, and found that there was a clear difference in gut microbiota composition between them. The microbiota that played a major role in the STm + PBS group were harmful *Enterobacterales* (Fig. 7L), while the STm + HBXN2020 group was *Candidatus_Saccharimonas* (Fig. 7L).

287 **Prophylactic *B. velezensis* HBXN2020 spores alleviated *S*. Typhimurium-**
288 **induced colitis.**

289 Based on the improved therapeutic efficacy of *B. velezensis* HBXN2020 in
290 the treatment of STm-induced colitis in mice, we further explored its potential
291 for disease prevention by evaluating pre-treatment. Mice in the PBS + STm
292 group and HBXN2020 + STm group were given the same amount of sterile
293 PBS and *B. velezensis* HBXN2020 spores by gavage one week in advance.
294 As shown in Fig. 8, compared with the PBS + STm group, oral administration
295 of *B. velezensis* HBXN2020 spores as a preventive measure remarkably
296 alleviated STm-induced colitis, including weight loss of mice ($P < 0.01$) (Fig.
297 8B), a significant reduction in DAI ($P < 0.001$) (the comprehensive score of
298 weight loss, stool consistency, and blood in the feces, Fig. 8C), and the
299 prevention of colon length shortening (Fig. 8D-E). However, the number of *B.*
300 *velezensis* HBXN2020 viable bacteria in feces is also gradually decreasing
301 with the time prolonging (Fig. S7A). Furthermore, compared with the PBS +
302 STm group, oral administration of *B. velezensis* HBXN2020 spores not only
303 reduced the number of STm in mouse feces (Fig. 8F) but also decreased
304 STm colonization in the ileum, cecum, and colon (Fig. 8G-H, S7B).

305 Histological analysis further revealed that oral administration of *B.*
306 *velezensis* HBXN2020 significantly reduced the infiltration of inflammatory
307 cells, mucosal damage and the overall histological score of colon tissue (Fig.
308 9A, S7C). Additionally, the mRNA expression levels of pro-inflammatory

309 cytokines, including TNF-α ($P < 0.05$), IL-1β ($P < 0.05$) and IL-6 ($P < 0.01$), in
310 the colon tissue of mice pretreated with *B. velezensis* HBXN2020 spores were
311 significantly decreased (Fig. 9B-D), while the mRNA levels of anti-
312 inflammatory cytokine (IL-10) were significantly higher ($P < 0.05$) (Fig. 9E)
313 than mice pretreated with PBS. In addition, compared to the group pretreated
314 with PBS, the group pretreated with *B. velezensis* HBXN2020 spores showed
315 a significant increase in mRNA expression levels of ZO-1 ($P < 0.001$), ocludin
316 ($P < 0.05$), and claudin ($P < 0.05$) in the colon tissue of mice (Fig. 9F-H).
317 While there was no significant difference in Muc2 expression (p=0.252) (Fig.
318 9I), the results were consistent with those of the therapeutic experiments.
319 Overall, these findings suggest that *B. velezensis* HBXN2020 can effectively
320 alleviate the symptoms of STm-induced colitis and the associated damage to
321 colon tissue.

322 Next, we examined the impact of prophylactic *B. velezensis* HBXN2020 on
323 the intestinal microbiota composition of STm-treated mice. Sobs, Chao1 index
324 and Shannon index have changed to some extent between groups, but
325 differences were not significant (Fig. 10A-C). Compared with the Control
326 group, the Simpson index significantly decreased in the PBS+STm group ($P <$
327 0.05, Fig. 10D). However, compared to the PBS+STm group, Simpson index
328 in the HBXN2020+STm group did not change (Fig. 10D). PCA analysis
329 showed a significant separation between control and PBS+STm groups, while
330 the HBXN2020+STm group, HBXN2020 group, and the control group were

clustered together (Fig. 10E). Next, we analyzed microbial community composition at the phylum and genus levels (Fig. 10F-G). At the phylum level, the PBS + STm group increased the abundance of *Bacteroidota*, *Proteobacteria*, *Actinobacteriota*, and *Deferribacterota* and reduced the abundance of *Verrucomicrobiota*, *Firmicutes*, *Patescibacteria*, and *Desulfobacterota* compared with the Control group(Fig. 10F, S8A). The HBXN2020 group increased the abundance of *Bacteroidota* compared to the control group. In contrast, compared to the PBS+STm group, the abundance of *Firmicutes* in the HBXN2020+STm group was significantly increased ($P < 0.05$). At the genus level, a depletion of *Lactobacillus* and *Akkermansia* (Fig. 10H-I) and an enrichment of *Alistipes*, *Bacteroides*, *Escherichia-Shigella*, *Alloprevotella*, *Helicobacter*, *Enterococcus*, and *Salmonella* were observed in PBS + STm group compared with the control (Fig. 10J-M, 8SB). The enrichment with *norank_f_Muribaculaceae* and *Alloprevotella* were observed in HBXN2020 group compared to the control. In contrast, an enrichment of *Lactobacillus*, *Akkermansia*, and *Lachnospiraceae_NK4A136_group* and a sharp decrease of *Alistipes*, *Bacteroides*, *Escherichia-Shigella*, and *Enterococcus* were observed in HBXN2020 + STm group compared to the PBS + STm group. LEfSe analysis showed that the abundance of *Lactobacillus* in the intestinal microbiota of mice was significantly increased after *B. velezensis* HBXN2020 treatment, while the abundance of harmful *Enterobacterales* in the untreated group was clearly increased (Fig. 10N).

Discussion

S. Typhimurium is an important intestinal pathogen that can cause invasive intestinal diseases such as bacterial colitis (18, 19). Although antibiotics are commonly used to treat bacterial-induced colitis, their overuse has significantly increased bacterial resistance in recent years, resulting in serious environmental pollution. A recent study showed that antibiotic-resistance genes in probiotics could be transmitted to the intestinal microbiota, which may threaten human health (20). Therefore, the source of probiotics is particularly important. Black pigs are an excellent domestic breed in China, with strong environmental adaptability and disease resistance (21). In this study, *B. velezensis* HBXN2020 was isolated from the free-range feces of black piglets in a mountain village in Xianning City (Hubei, China) and exhibited excellent antibacterial activity. Previous studies have demonstrated that the difficidins isolated from *B. subtilis* can inhibit bacterial protein synthesis, giving it broad-spectrum antibacterial activity against *Gram positive* and *Gram negative* bacteria. Therefore, we speculate that *B. velezensis* HBXN2020 has the ability to synthesize Difficidin or its derivatives (22). Otherwise, *in vitro* tolerance assays showed that *B. velezensis* HBXN2020 spores have good tolerance to high temperature, strong acids, bile salts, and simulated gastric and intestinal fluid, which was similar to previous research results (23). Furthermore, antibiotic susceptibility tests showed that *B.*

375 *velezensis* HBXN2020 does not exhibit antibiotic resistance.

376 Probiotics are unique in that they are alive when consumed, and unlike food
377 or drug, they have the potential to produce toxins or infections in the body (24,
378 25). Therefore, assessing the biosafety of probiotics is crucial. In this study,
379 the safety of *B. velezensis* HBXN2020 was evaluated by measuring the body
380 weight, intestinal barrier proteins, and inflammatory cytokines of the
381 experimented mice, as well as conducting routine blood and biochemical tests.
382 The results showed that the expression levels of ZO-1 and occludin in the
383 colon of mice increased after treatment with different doses of *B. velezensis*
384 HBXN2020 spores. It has been reported that ZO-1, occludin and claudin are
385 the three most important tight junction proteins in intercellular connections,
386 which play a crucial role in maintaining the intestinal epithelial barrier (26, 27).
387 Therefore, upregulating the expression levels of ZO-1 and Occludin might
388 enhance intestinal barrier function.

389 Alanine aminotransferase (ALT) and aspartate aminotransferase (AST) are
390 important aminotransferases in animals and are considered key parameters
391 for evaluating liver function injury (28, 29). Under normal circumstances, the
392 levels of ALT and AST are in dynamic balance without notable changes.
393 However, when the liver is damaged or becomes dysfunctional, the levels of
394 aminotransferases (ALT and AST) increase significantly (30). Previous
395 studies have shown that CCL4-induced liver injury strongly increases plasma
396 ALT/AST levels (31). Zhang et al. reported that the addition of *Bacillus subtilis*

397 to chicken diets significantly decreased the serum levels of ALT and AST (32).
398 In this present study, the levels of ALT and AST in the probiotic-treated group
399 were slightly lower than those in the control group, indicating that *B.*
400 *velezensis* HBXN2020 had no negative effect on liver health in mice.
401 Furthermore, routine blood tests found that the blood indices of the *B.*
402 *velezensis* HBXN2020 treatment group were within the normal reference
403 range, similar to that of the control group.

404 To further evaluate the potential of *B. velezensis* HBXN2020 spores in
405 alleviating *S.* Typhimurium-induced colitis, mice were challenged with *S.*
406 Typhimurium ATCC14028 and then treated with *B. velezensis* HBXN2020
407 spores via oral administration. Our experimental results demonstrated that
408 oral treatment with *B. velezensis* HBXN2020 spores could alleviate *S.*
409 Typhimurium-induced colitis, as evidenced by decreased weight loss, DAI,
410 and histological damage, which is similar with prior studies (33, 34). Previous
411 research showed that macrophages are the first line of host defense against
412 bacterial infection. They release pro-inflammatory cytokines, which are critical
413 in initiating adaptive immune responses (35, 36). Nevertheless, pro-
414 inflammatory cytokines have immunological properties that can be beneficial
415 for the host to resist the invasion of bacteria and other microbes in the
416 surrounding environment (37). For instance, pre-treatment with recombinant
417 murine TNF-α was shown to protect mice against lethal bacterial (*E. coli*)
418 infection (38). PJ-34 exerted protective effects on intestinal epithelial cells

419 against invasive *Salmonella* infection by upregulating IL-6 expression through
420 the ERK and NF-κB signal pathways (39). However, some studies have
421 shown that excessive immune cell activation can lead to tissue damage, multi-
422 organ malfunction, systemic or chronic inflammation, and autoimmune
423 disorders (40, 41). IL-10 is a recognized anti-inflammatory mediator that plays
424 a crucial role in maintaining intestinal microbe-immune homeostasis,
425 regulating the release of inflammatory mediators, and inhibiting pro-
426 inflammatory responses of innate and adaptive immunity (42-44). For instance,
427 previous studies have shown that *Clostridium butyrate* can induce the
428 production of IL-10 in the intestine, thereby alleviating experimental colitis in
429 mice (45). Similar results were observed in our study, where oral
430 administration of *B. velezensis* HBXN2020 spores reduced the expression
431 levels of TNF-α, IL-1β and IL-6 while increasing the levels of IL-10 in the colon
432 of mice. Furthermore, oral administration of *B. velezensis* HBXN2020 spores
433 improved the functional damage and integrity of the intestinal barrier caused
434 by *S.* Typhimurium infection, as evidenced by the upregulated expression
435 levels of intestinal barrier proteins and reduced histological damage.

436 Subsequently, we further analyzed the colon microbiome and it was
437 noteworthy that oral *B. velezensis* HBXN2020 markedly increased alpha
438 diversity of the colonic microbiota. As reported in prior studies, elevated alpha
439 diversity associates with enhanced anti-interference ability (46). PCA analysis
440 results showed that oral administration of *B. velezensis* HBXN2020

significantly affected the structure of the intestinal microbiota. Further analysis at the phylum/genus level revealed that *B. velezensis* HBXN2020 treatment reduced the increase of *Bacteroides*, *Escherichia-Shigella*, and *Salmonella* (harmful to intestinal homeostasis) in colitis (47), but enhanced the relative abundance of *Lactobacillus* (known for enhancing the epithelial barrier by increasing mucus secretion and upregulating the expression of tight junction proteins such as claudin-1, occludin, and ZO-1) (48) and *Akkermansia* (known for modulating intestinal immune response by producing short chain fatty acids and reducing the secretion of pro-inflammatory cytokines) (49). *Bacteroides* is generally 'friendly' commensals in the intestine, but they can enter normal tissues through the intestinal mucosa when intestinal barrier function becomes compromised (50), leading to inflammation, diarrhea, and abdominal abscess (51). *Escherichia-Shigella* is a common intestinal pathogen, and its relative abundance is associated with pro-inflammatory states (52). *Salmonella* can secrete bacterial virulence proteins, which are directly delivered to the host cell cytosol through the Type III secretion system and induce the expression of pro-inflammatory cytokines (53), leading to inflammation. Overall, the structure of the colon microbiota was disrupted by *S*. Typhimurium ATCC14028 infection and increased the relative abundance of harmful bacteria, while therapeutic *B. velezensis* HBXN2020 enhanced the abundance of beneficial bacteria, reduced inflammation, and improved intestinal barrier function.

Due to the improved efficacy of treating *S.* Typhimurium-induced colitis, we further investigated the potential of *B. velezensis* HBXN2020 spores for disease prevention by evaluating pre-treatment. Similarly to the therapeutic effect of oral *B. velezensis* HBXN2020, pre-treatment with *B. velezensis* HBXN2020 spores effectively alleviated the symptoms of *S.* Typhimurium-induced colitis and reduced the expression levels of pro-inflammatory cytokines and increased anti-inflammatory cytokine levels in the colon of *S.* Typhimurium-infected mice. Furthermore, pre-treatment with *B. velezensis* HBXN2020 spores also promoted the expression levels of intestinal barrier proteins in the colon of *S.* Typhimurium-infected mice. In addition, the microbiota composition was also dramatically modulated by prophylactic *B. velezensis* HBXN2020 in mice with colitis, although the community richness and diversity revealed by alpha diversity index was not significantly impacted in mice with colitis by prophylactic-treatment. Further analysis at the genus level revealed that prophylactic *B. velezensis* HBXN2020 clearly increased SCFAs-producing bacteria including *Lactobacillus* and *Akkermansia*, which was consistent with the results of therapeutic *B. velezensis* HBXN2020. Similarly, harmful bacteria such as *Alistipes*, *Bacteroides*, *Escherichia-Shigella*, and *Enterococcus* were significantly enriched in the PBS+STm group. *Alistipes* is a facultative - pathogenic bacteria and promotes the development of inflammation, obesity, and colorectal cancer (54). Based on those results, we found that prophylactic *B. velezensis* HBXN2020 alleviates

485 *S.* Typhimurium induced colitis by increasing the abundance of beneficial
486 bacteria, attenuating pro-inflammatory response of the intestine, and
487 increasing intestinal barrier function.
488

489 **Conclusion**

490 In conclusion, infection with *S.* Typhimurium ATCC14028 disrupts the
491 intestinal mucosal barrier, and leading to intestinal inflammation. Both
492 therapeutic and prophylactic, supplementing *B. velezensis* HBXN2020 spores
493 alleviates *S*. Typhimurium-induced colonic injury by reducing Salmonella
494 colonization, and enhancing the abundance of beneficial bacteria (especially
495 *Lactobacillus* and *Akkermansia*) and intestinal barrier integrity, and
496 decreasing inflammation.
497

498 **Experimental procedures**

499 **Animals and bacterial strains.**

500 Female specific-pathogen-free (SPF) C57BL/6 mice aged 6 to 8 weeks
501 were purchased from the Animal Experimental Center of Huazhong
502 Agricultural University. All mice experiments were conducted in the standard
503 SPF facility of Huazhong Agricultural University, with 12 h of light and 12 h of
504 darkness at a temperature of 25°C and ad libitum access to food and water.
505 The use of animals in this experiment was approved by the Animal Care and

506 Ethics Committee of Huazhong Agricultural University (Ethics Approval
507 Number: HZAUMO-2023-0089).

508 The strains used in this study are listed in Table S2, and all the primers
509 used in Table S3. *Clostridium perfringens* were cultured in a fluid thioglycollate
510 medium (FTG) (Hopebio, Qingdao, China) at 45°C. *Streptococcus suis*,
511 *Pasteurella multocida*, and *Actinobacillus pleuropneumoniae* were cultured in
512 tryptic soy broth (TSB) (BD Biosciences, MD, United States) medium
513 supplemented with 5% (v/v) sheep serum (Solarbio, Beijing, China) at 37°C,
514 while the other bacterial strains were cultured in Luria Bertani (LB) medium
515 (Solarbio, Beijing, China) at 37°C. In addition, the Difco sporulation medium
516 (DSM) was used for inducing the sporulation of *B. velezensis* HBXN2020 via
517 the nutrient depletion method (55).

518

519 **Stain isolation, growth conditions and strain identification.**

520 In this study, we isolated 362 *Bacillus* strains from the feces of healthy
521 black piglets that were free-ranging in a mountain village in Xianning City,
522 Hubei Province, China, and 4 *Bacillus* strains were screened through initial
523 antibacterial tests. Then, a strain with broad-spectrum antimicrobial activity
524 was ultimately screened out by the antibacterial spectrum assay (Table S4),
525 and named as *B. velezensis* HBXN2020. The strain was stored in 28%
526 glycerol at −80°C. For culturing the bacterial cells, Luria-Bertani (LB) media or
527 agar plates supplemented with 1.5% agar were used and incubated at 37°C.

528 A single bacterial colony was inoculated into 10 mL of LB medium and
529 incubated overnight at 37°C with shaking (180 rpm). Then, the 16S rRNA
530 sequence was amplified by the polymerase chain reaction (PCR) using
531 forward primer 27F and reverse primer 1492R and similarity analysis with the
532 National Center for Biotechnology Information (NCBI) alignment tool (BLAST)
533 was used to identify the species.
534

535 **Genome sequencing, annotation and analysis**

536 The complete genome of *B. velezensis* HBXN2020 was sequenced using
537 the Illumina HiSeq PE and PacBio RSII (SMRT) platforms (Shanghai Majorbio
538 Bio-pharm Technology Co., Ltd.). Briefly, the short reads from the Illumina
539 HiSeq PE were assembled into contigs using SPAdenovo
540 (http://soap.genomics.org.cn/). The long reads from the PacBio RSII and the
541 Illumina contigs were then aligned using the miniasm and Racon tools in
542 Unicycler (version 0.4.8, https://github.com/rrwick/Unicycler) to generate long-
543 read sequences. During the assembly process, sequence correction was
544 performed using Pilon (version 1.22,
545 https://github.com/broadinstitute/pilon/wiki/Standard-Output). Lastly, a
546 complete genome with seamless chromosomes was obtained.

547 The coding sequences (CDs) of the *B. velezensis* HBXN2020 genome were
548 predicted using Glimmer (version 3.02,
549 http://ccb.jhu.edu/software/glimmer/index.shtml). The tRNA and rRNA genes

550 were predicted using TRNAscan-SE (version 2.0,
551 http://trna.ucsc.edu/software/) and Barrnap (version 0.8,
552 https://github.com/tseemann/barrnap), respectively. The functional annotation
553 of all CDSs was performed using various databases, including Swiss-Prot
554 Database (https://web.expasy.org/docs/swiss-prot_guideline.html), Pfam
555 Database (http://pfam.xfam.org/), EggNOG Database (http://eggnog.embl.de/),
556 GO Database (http://www.geneontology.org/), and KEGG Database
557 (http://www.genome.jp/kegg/). The circular map of the *B. velezensis*
558 HBXN2020 genome was generated using CGView (version 2,
559 http://wishart.biology.ualberta.ca/cgview/) (56).
560

561 **Comparative genomic analysis**

562 To elucidate the phylogenetic relationships from a whole-genome
563 perspective, a phylogenetic tree based on the whole genome was constructed
564 using the Type (Strain) Genome Server (TYGS) online (https://ggdc.dsmz.de/)
565 (57). The average nucleotide identity (ANI) values of genome to genome were
566 calculated using the JSpeciesWS online service (58), and a heatmap was
567 then generated using TBtools (version 1.113) (59).

568 **Growth curves of *B. velezensis* HBXN2020**

569 The growth curve of *B. velezensis* HBXN2020 was recorded in flat-
570 bottomed 100-well microtiter plates via detecting optical density at 600 nm
571 (OD_{600}) at 1 h intervals using the automatic growth curve analyzer (Bioscreen,

572 Helsinki, Finland).

573

574 **Antimicrobial Assays**

575 The *in vitro* antagonistic activity of *B. velezensis* HBXN2020 was tested
576 using the agar well-diffusion method against 18 indicator strains (pathogens),
577 which included 7 standard strains (*E. coli* ATCC 25922, *E. coli* ATCC 35150,
578 *S.* Typhimurium ATCC 14028 (STm), *S.* Typhimurium SL1344, *S. aureus*
579 ATCC 29213, *S. aureus* ATCC 43300, and *C. perfringens* CVCC 2030) and
580 11 clinical isolates (*E. coli* EC024, *S.* Enteritidis SE006, *S. aureus* S21, *C.*
581 *perfringens* CP023, *C. perfringens* CP002, *S. suis* SC19, *S. suis* SS006, *P.*
582 *multocida* PM002, *P. multocida* PM008, *A.* pleuropneumoniae APP015, and *A.*
583 pleuropneumoniae APP017). All plates were cultured at 37°C for 16 h before
584 observing the inhibition zone, and the diameter of the inhibition zone was
585 measured using a vernier caliper. The presence of a clear zone indicated
586 antagonistic activity.

587

588 **Antibiotic susceptibility assays**

589 Antimicrobial susceptibility testing was performed using the Kirby-Bauer
590 (KB) disk diffusion method in accordance with the Clinical Laboratory
591 Standards Institute (CLSI) guidelines (60). The antimicrobial agents tested
592 were: Ampicillin, Meropenem, Piperacillin, Gentamycin, Tetracycline,
593 Doxycycline, Minocycline, Erythromycin, Enrofloxacin, Ofloxacin,

594 Sulfamethoxazole, Trimethoprim-sulfamethoxazole, Polymyxin B, Teicoplanin,
595 Trimethoprim, Florfenicol, Spectinomycin, Nitrofurantoin, and Rifampicin. The
596 diameter of the inhibition zone was measured using a vernier caliper.
597

598 ***In vitro* resistance assay of *B. velezensis* HBXN2020**

599 *B. velezensis* HBXN2020 spores (100 μL) or vegetative cells (100 μL) were
600 separately resuspended in 900 μL of LB medium supplemented with different
601 pH values (2, 3, 4, 5 or 6), bile salts (0.85% NaCl, 0.3%), simulated gastric
602 fluid (SGF, HCl, pH 1.2) containing 10 g L^{-1} of pepsin in 0.85% NaCl solution,
603 or simulated intestinal fluid (SIF, NaOH, pH 6.8) containing 10 g L^{-1} of trypsin
604 in 0.05 M KH2PO4 solution, and incubated at 37 °C. A normal LB medium (pH
605 7.0) was used as the control. At predetermined time points, 100 μL was taken
606 from each sample, serially diluted 10-fold with sterile PBS (pH 7.2), and then
607 spread onto LB agar plates. The plates were incubated overnight in a
608 constant temperature incubator at 37°C, and the bacterial colonies were
609 counted. The survival rate was calculated using the following formula: Survival
610 rate = (number of bacteria in the treatment group/number of bacteria in the
611 control group) × 100%.

612 One milliliter of *B. velezensis* HBXN2020 spores or vegetative cells were
613 separately placed in water baths at different temperatures (37°C, 45°C, 55°C,
614 65°C, 75°C, 85°C or 95°C) for 20 min, with a 37°C water bath used as the
615 control. The survival rate was calculated as described above.

616

617 ***In vitro* bacterial competition.**

618 To investigate whether *B. velezensis* HBXN2020 directly inhibited the
619 growth of STm, we performed spot-on lawn and agar-well diffusion assays, as
620 well as co-culture assays in liquid culture medium. In the spot-on lawn
621 antimicrobial assays, we prepared double layers of agar by first pouring LB
622 agar into the plate as the bottom layer. The top layer consisted of 10 mL TSB
623 broth containing 0.7% agar with STm overnight culture. Then, 10 μL of *B.*
624 *velezensis* HBXN2020 overnight culture and cell-free supernatant (CFS) were
625 respectively spotted onto TSB agar and incubated at 37°C for 12 h to
626 measure the inhibition zone. A transparent zone of at least 1 mm around the
627 spot was considered positive.

628 The antagonistic effect of *B. velezensis* HBXN2020-CFS against STm was
629 determined using the agar-well diffusion assays. To collect *B. velezensis*
630 HBXN2020-CFS, the culture was centrifuged at 9,000g for 15 min at 4°C, and
631 the supernatant was filtered through a 0.22 μm membrane filter (Millipore,
632 USA). The STm lawn medium was prepared by mixing 10 mL of TSB broth
633 containing 0.7% agar with STm overnight culture and then poured into a
634 sterile plate covered with LB agar and Oxford cups, 8 mm diameter wells were
635 prepared in the TSB agar after removing the cups. The wells were filled with
636 100 μL of *B. velezensis* HBXN2020-CFS, LB medium or ampicillin (100 μg
637 mL^{-1}). The plates were incubated at 37°C for 14 h, and the inhibition zone was

638 measured.

639 The co-culture assay was conducted by incubating *B. velezensis*
640 HBXN2020 and *S.* Typhimurium ATCC14028 (carry pET28a (+), kanamycin
641 resistance) (33) separately overnight at 37°C and diluting them to 10^4
642 CFU/mL. Then, the two strains were mixed at different ratios (1:1, 1:10, 1:50
643 or 1:100) and co-cultured at 37°C with shaking (180 rpm). At predetermined
644 time points, serial 10-fold dilutions were prepared for all samples and spread
645 onto selective (kanamycin 50 μg mL^{-1}) LB agar plates and cultured at 37°C for
646 12 h before bacterial counting. Viable colony counts ranged from 30 to 300
647 per plate.

648

649 **Biosafety assessment**

650 After a 7-day acclimation period (free access to water and food), mice were
651 randomly divided into four treatment groups (n = 5): low-dose *B. velezensis*
652 HBXN2020 spores group (L-HBXN2020 group, 10^7 CFU/mouse), medium-
653 dose *B. velezensis* HBXN2020 spores group (M-HBXN2020 group, 10^8
654 CFU/mouse), high-dose *B. velezensis* HBXN2020 spores group (H-
655 HBXN2020 group, 10^9 CFU/mouse), and a control group. During the
656 experimental period (15 days), mice were weighed and orally gavaged with
657 their respective treatments once every two days. On day 15, all mice were
658 euthanized, and blood, heart, liver, spleen, lung, kidney, ileum, cecum, and
659 colon were collected. Blood samples were used for routine blood and

660 biochemistry tests. Major organ tissues (heart, liver, spleen, lung, and kidney)
661 and a 5-mm distal segment of the colon were used for histopathology. The
662 remaining colonic tissues were rapidly frozen in liquid nitrogen and stored at
663 −80°C for cytokine and tight junction protein expression analysis.
664

665 ***Salmonella* Typhimurium-induced mouse model of colitis.**

666 After 7 days of acclimation (free access to water and food), mice were
667 randomly divided into three treatment groups (n = 8): Control group, STm +
668 PBS group, and STm + HBXN2020 group. The *S.* Typhimurium-induced colitis
669 was performed as previously described (61), with slight modifications. On the
670 first day of the experiment, all mice in the STm + PBS group and STm +
671 HBXN2020 group were orally inoculated with 200 μL (5×10^7 CFU/mouse) of
672 STm. On days 1, 3 and 5 following STm infection, each mouse in the STm +
673 HBXN2020 group received 200 μL (1×10^8 CFU/mouse) of *B. velezensis*
674 HBXN2020 spores via gavage administration. In contrast, the control group
675 and STm + PBS group received 200 μL of sterile PBS by oral gavage. Fecal
676 samples were collected daily following STm infection and resuspended in
677 sterile PBS. The number of STm in mice feces from both the STm + PBS and
678 STm + HBXN2020 groups was then determined by spreading a serial 10-fold
679 dilution on selective LB agar plates containing 50 μg mL^{-1} kanamycin.
680 Throughout the entire experiment, the body weight, stool consistency and
681 fecal occult blood of all mice were monitored daily. As shown in Table S5,

682 disease activity index (DAI) was calculated by the sum of the scores from
683 three parameters (62). On day 7 after STm infection, all mice were euthanized,
684 their ileum, cecum and colon were collected. The length of colon was
685 measured, and a 5-mm distal segment of the colon was fixed in 4%
686 paraformaldehyde for further histopathology. The remaining colon was then
687 rapidly frozen in liquid nitrogen and stored at −80°C for cytokine and tight
688 junction protein expression analysis. Then, the number of STm in the ileum,
689 cecum, and colon was determined by spreading serial 10-fold dilutions on
690 selective LB agar plates.

691 To investigate the prophylactic efficacy of *B. velezensis* HBXN2020 in
692 ameliorating STm-induced colitis, another independent experiment was
693 conducted using six-week-old female C57BL/6 mice (SPF). After a seven-day
694 acclimation period, mice were randomly assigned to three groups (n = 8):
695 control group, PBS + STm group and HBXN2020 + STm group. On days 1, 3,
696 5 and 7, each mouse in the HBXN2020 + STm group received 200 μL (1×10^8
697 CFU/mouse) of *B. velezensis* HBXN2020 spores via gavage administration.
698 Meanwhile, mice in the control group and PBS + STm group received 200 μL
699 of sterile PBS by oral gavage. On day 7, all mice in the PBS + STm group and
700 HBXN2020 + STm group were orally inoculated with 200 μL (5×10^7
701 CFU/mouse) of STm. Fecal samples were collected daily following STm
702 infection from both groups and resuspended in sterile PBS. The number of
703 STm in the feces of mice was then determined by spreading serial 10-fold

704 dilutions on selective LB agar plates (50 μg mL^{-1} kanamycin). Throughout the
705 entire experiment, the body weight and DAI scores of all mice were monitored
706 daily. On day 12, all mice were euthanized, and the ileum, cecum, and colon
707 were collected. The colon length was measured, and a 5-mm distal segment
708 of the colon was fixed in 4% formalin for sectioning and staining. The
709 remaining colon was stored at −80°C for future analysis. Lastly, the number of
710 STm in the ileum, cecum, and colon was determined using a selective LB
711 agar plate.
712

713 **Determination of cytokines and tight junction protein expression in**
714 **colon tissue**

715 Total RNA was extracted from colon tissues using TRIpure reagent (Aidlab,
716 China), and cDNA was obtained using HiScript® III RT SuperMix for qPCR
717 (+gDNA wiper) (Vazyme, China). RT-qPCR for each gene was performed in
718 triplicate using qPCR SYBR Green Master Mix (Yeasen Biotechnology,
719 Shanghai, China). The relative expression level of cytokine and tight junction
720 protein genes was calculated using the $2^{-\Delta\Delta Ct}$ method with β-actin and
721 GAPDH as reference genes. The primer sequences used in the RT-qPCR test
722 are listed in Table S3.
723

724 **Histopathology analysis**

725 Colon tissue samples (0.5 cm) were fixed in 4% paraformaldehyde for 24 h,

726 and the fixed tissues were then embedded in paraffin and sectioned. The
727 sections were stained with hematoxylin and eosin (H&E) and observed and
728 imaged using an optical microscope (Olympus Optical, Tokyo, Japan). The
729 histopathological score included the degree of inflammatory infiltration,
730 changes in crypt structures, and the presence or absence of ulceration and
731 edema. The scoring criteria were determined as previously described (34).
732

733 **16S rRNA gene sequencing and analysis**

734 According to the manufacturer's instructions, colon microbial community
735 genomes were extracted using E.Z-N.A ® Stool DNA Kit (Omega; D4015-01),
736 and quality was detected by 1% agarose gel electrophoresis. The 16S rRNA
737 V3-V4 variable region was amplified by PCR using universal primers 338F (5
738 '- ACTCCTACGGGGGGCAG-3') and 806R (5 '-
739 GACTACHVGGGTWTCTAAT-3'). The PCR products were examined by
740 electrophoresis on 2% agarose gels and then purified with the AxyPrep DNA
741 gel extraction kit (Axygen Biosciences, USA). A sequencing library was
742 constructed using the NEXTFLEX® Rapid DNA-Seq Kit, and sequencing was
743 performed using the Illumina MiSeq platform. Raw reads were quality
744 evaluated and filtered by fastp (version 0.20.0) and merged using FLASH
745 (version 1.2.7). The optimized sequences were clustered into operational
746 taxonomic units (OTUs) based on 97% sequence similarity using UPARSE
747 (version 7.1). The representative sequences of each OTU was classified by

RDP classifier (version 2.2; confidence threshold value, 0.7). Alpha diversity was assessed using the ACE, chao, Shannon, and Simpson indices. The β-diversity analysis was performed using Bray-Curtis distances and visualized through principal component analysis (PCA). Linear discriminant analysis (LDA) effect size (LefSe) was used to identify differential microbiota between groups.

Statistical Analysis

Statistical analysis was performed using GraphPad Prism 8.3.0 (GraphPad Software, San Diego, CA, USA) and Excel (Microsoft, Redmond, USA). Data are presented as mean ± standard error of the mean (SEM). Differences between two groups were evaluated using two-tailed unpaired Student's t-test, and all other comparisons were conducted using one-way analysis of variance (ANOVA) with Tukey's multiple comparisons test. For all analyses, significance differences are denoted as: *, $P < 0.05$, **, $P < 0.01$, and ***, $P < 0.001$.

Data availability

The complete genome sequence of *Bacillus velezensis* HBXN2020 has been deposited in GenBank and assigned accession numbers: CP119399.1

Conflict of interest: We declare no conflict of interest.

ACKNOWLEDGMENTS

This work was supported by grants from the National Program on Key Research Project of China (2021YFD1800300, 2022YFD1800800), “Yingzi Tech & Huazhong Agricultural University Intelligent Research Institute of Food Health” (No. IRIFH202209; IRIFH202301), and the Fundamental Research Funds for the Central Universities (2662016PY004).

Author contributions

Linkang Wang: Conceptualization, Methodology, Data curation, Formal analysis, Writing - original draft. **Haiyan Wang, Xinxin Li, Mengyuan Zhu**: Methodology, Data curation, Planned and performed the experiments. **Dongyang Gao, Dayue Hu, Zhixuan Xiong**: Methodology, Writing - Reviewing and Editing. **Xiangmin Li**: Supervision, Writing-reviewing and editing. **Ping Qian**: Conceptualization, Funding acquisition, Project administration, Supervision, Writing-Reviewing and Editing. All authors read and approved the submitted version of the paper.

Funding information

This work was supported by grants from the National Program on Key Research Project of China (2021YFD1800300, 2022YFD1800800), “Yingzi Tech & Huazhong Agricultural University Intelligent Research Institute of Food

Health" (No. IRIFH202209; IRIFH202301), and the Fundamental Research Funds for the Central Universities (2662016PY004).

Reference

1. Fabrega A, Vila J. 2013. Salmonella enterica serovar Typhimurium skills to succeed in the host: virulence and regulation. Clin Microbiol Rev 26:308-41.
2. Yang WH, Westman JS, Heithoff DM, Sperandio M, Cho JW, Mahan MJ, Marth JD. 2021. Neu3 neuraminidase induction triggers intestinal inflammation and colitis in a model of recurrent human food-poisoning. Proc Natl Acad Sci U S A 118.
3. Katiyo S, Muller-Pebody B, Minaji M, Powell D, Johnson AP, De Pinna E, Day M, Harris R, Godbole G. 2019. Epidemiology and Outcomes of Nontyphoidal Salmonella Bacteremias from England, 2004 to 2015. J Clin Microbiol 57.
4. Mohan A, Munusamy C, Tan YC, Muthuvelu S, Hashim R, Chien SL, Wong MK, Khairuddin NA, Podin Y, Lau PS, Ng DC, Ooi MH. 2019. Invasive Salmonella infections among children in Bintulu, Sarawak, Malaysian Borneo: a 6-year retrospective review. BMC Infect Dis 19:330.
5. Ferri M, Ranucci E, Romagnoli P, Giaccone V. 2017. Antimicrobial resistance: A global emerging threat to public health systems. Crit Rev Food Sci Nutr 57:2857-2876.
6. Paulson JA, Zaoutis TE, Council on Environmental H, Committee on Infectious D. 2015. Nontherapeutic Use of Antimicrobial Agents in Animal Agriculture: Implications for Pediatrics. Pediatrics 136:e1670-7.
7. Reyman M, van Houten MA, Watson RL, Chu M, Arp K, de Waal WJ, Schiering I, Plotz FB, Willems RJL, van Schaik W, Sanders EAM, Bogaert D. 2022. Effects of early-life antibiotics on the developing infant gut microbiome and resistome: a randomized trial. Nat Commun 13:893.
8. Cristofori F, Dargenio VN, Dargenio C, Miniello VL, Barone M, Francavilla R. 2021. Anti-Inflammatory and Immunomodulatory Effects of Probiotics in Gut Inflammation: A Door to the Body. Front Immunol 12:578386.
9. Wang Y, Xie Q, Zhang Y, Ma W, Ning K, Xiang JY, Cui J, Xiang H. 2020. Combination of probiotics with different functions alleviate DSS-induced colitis by regulating intestinal microbiota, IL-10, and barrier function. Appl Microbiol Biotechnol 104:335-349.
10. Ohland CL, Macnaughton WK. 2010. Probiotic bacteria and intestinal epithelial barrier function. Am J Physiol Gastrointest Liver Physiol 298:G807-19.
11. Gu SB, Zhao LN, Wu Y, Li SC, Sun JR, Huang JF, Li DD. 2015. Potential probiotic attributes of a new strain of Bacillus coagulans CGMCC 9951 isolated from healthy piglet feces. World J Microbiol Biotechnol 31:851-63.
12. Ouattara HG, Reverchon S, Niamke SL, Nasser W. 2017. Regulation of the synthesis of pulp degrading enzymes in Bacillus isolated from cocoa fermentation. Food Microbiol 63:255-262.
13. Abdhul K, Ganesh M, Shanmughapriya S, Vanithamani S, Kanagavel M, Anbarasu K, Natarajaseenivasan K. 2015. Bacteriocinogenic potential of a probiotic strain Bacillus coagulans [BDU3] from Ngari. Int J Biol Macromol 79:800-6.

832 14. Ye M, Tang X, Yang R, Zhang H, Li F, Tao F, Li F, Wang Z. 2018. Characteristics and Application
833 of a Novel Species of Bacillus: Bacillus velezensis. ACS Chem Biol 13:500-505.
834 15. Shao J, Liu Y, Xie J, Stefanic P, Lv Y, Fan B, Mandic-Mulec I, Zhang R, Shen Q, Xu Z. 2022.
835 Annulment of Bacterial Antagonism Improves Plant Beneficial Activity of a Bacillus velezensis
836 Consortium. Appl Environ Microbiol 88:e0024022.
837 16. Li A, Wang Y, Li Z, Qamar H, Mehmood K, Zhang L, Liu J, Zhang H, Li J. 2019. Probiotics
838 isolated from yaks improves the growth performance, antioxidant activity, and cytokines
839 related to immunity and inflammation in mice. Microb Cell Fact 18:112.
840 17. Zhang DX, Kang YH, Zhan S, Zhao ZL, Jin SN, Chen C, Zhang L, Shen JY, Wang CF, Wang GQ,
841 Shan XF, Qian AD. 2019. Effect of Bacillus velezensis on Aeromonas veronii-Induced Intestinal
842 Mucosal Barrier Function Damage and Inflammation in Crucian Carp (Carassius auratus).
843 Front Microbiol 10:2663.
844 18. Herp S, Brugiroux S, Garzetti D, Ring D, Jochum LM, Beutler M, Eberl C, Hussain S, Walter S,
845 Gerlach RG, Ruscheweyh HJ, Huson D, Sellin ME, Slack E, Hanson B, Loy A, Baines JF, Rausch P,
846 Basic M, Bleich A, Berry D, Stecher B. 2019. Mucispirillum schaedleri Antagonizes Salmonella
847 Virulence to Protect Mice against Colitis. Cell Host Microbe 25:681-694 e8.
848 19. Schultz BM, Paduro CA, Salazar GA, Salazar-Echegarai FJ, Sebastian VP, Riedel CA, Kalergis AM,
849 Alvarez-Lobos M, Bueno SM. 2017. A Potential Role of Salmonella Infection in the Onset of
850 Inflammatory Bowel Diseases. Front Immunol 8:191.
851 20. Crits-Christoph A, Hallowell HA, Koutouvalis K, Suez J. 2022. Good microbes, bad genes? The
852 dissemination of antimicrobial resistance in the human microbiome. Gut Microbes
853 14:2055944.
854 21. Yang W, Liu Z, Zhao Q, Du H, Yu J, Wang H, Liu X, Liu H, Jing X, Yang H, Shi G, Zhou L, Liu J.
855 2022. Population Genetic Structure and Selection Signature Analysis of Beijing Black Pig.
856 Front Genet 13:860669.
857 22. Kaspar F, Neubauer P, Gimpel M. 2019. Bioactive Secondary Metabolites from Bacillus subtilis:
858 A Comprehensive Review. J Nat Prod 82:2038-2053.
859 23. Du H, Yao W, Kulyar MF, Ding Y, Zhu H, Pan H, Li K, Bhutta ZA, Liu S, Li J. 2022. Effects of
860 Bacillus amyloliquefaciens TL106 Isolated from Tibetan Pigs on Probiotic Potential and
861 Intestinal Microbes in Weaned Piglets. Microbiol Spectr 10:e0120521.
862 24. Sanders ME, Akkermans LM, Haller D, Hammerman C, Heimbach J, Hormannsperger G, Huys
863 G, Levy DD, Lutgendorff F, Mack D, Phothirath P, Solano-Aguilar G, Vaughan E. 2010. Safety
864 assessment of probiotics for human use. Gut Microbes 1:164-85.
865 25. Snydman DR. 2008. The safety of probiotics. Clin Infect Dis 46 Suppl 2:S104-11; discussion
866 S144-51.
867 26. Bazzoni G, Martinez-Estrada OM, Orsenigo F, Cordenonsi M, Citi S, Dejana E. 2000. Interaction
868 of junctional adhesion molecule with the tight junction components ZO-1, cingulin, and
869 occludin. J Biol Chem 275:20520-6.
870 27. Zihni C, Mills C, Matter K, Balda MS. 2016. Tight junctions: from simple barriers to
871 multifunctional molecular gates. Nat Rev Mol Cell Biol 17:564-80.
872 28. Gou S, Chen N, Wu X, Zu M, Yi S, Ying B, Dai F, Ke B, Xiao B. 2022. Multi-responsive
873 nanotheranostics with enhanced tumor penetration and oxygen self-producing capacities for
874 multimodal synergistic cancer therapy. Acta Pharm Sin B 12:406-423.
875 29. Ozer J, Ratner M, Shaw M, Bailey W, Schomaker S. 2008. The current state of serum

876 biomarkers of hepatotoxicity. Toxicology 245:194-205.
877 30. Tang Y, Gao C, Xing M, Li Y, Zhu L, Wang D, Yang X, Liu L, Yao P. 2012. Quercetin prevents
878 ethanol-induced dyslipidemia and mitochondrial oxidative damage. Food Chem Toxicol
879 50:1194-200.
880 31. Singhal M, Liu X, Inverso D, Jiang K, Dai J, He H, Bartels S, Li W, Abdul Pari AA, Gengenbacher
881 N, Besemfelder E, Hui L, Augustin HG, Hu J. 2018. Endothelial cell fitness dictates the source
882 of regenerating liver vasculature. J Exp Med 215:2497-2508.
883 32. Zhang L, Bai K, Zhang J, Xu W, Huang Q, Wang T. 2017. Dietary effects of Bacillus subtilis fmbj
884 on the antioxidant capacity of broilers at an early age. Poult Sci 96:3564-3573.
885 33. Cao Z, Wang X, Pang Y, Cheng S, Liu J. 2019. Biointerfacial self-assembly generates lipid
886 membrane coated bacteria for enhanced oral delivery and treatment. Nat Commun 10:5783.
887 34. Wu J, Lin Z, Wang X, Zhao Y, Zhao J, Liu H, Johnston LJ, Lu L, Ma X. 2022. Limosilactobacillus
888 reuteri SLZX19-12 Protects the Colon from Infection by Enhancing Stability of the Gut
889 Microbiota and Barrier Integrity and Reducing Inflammation. Microbiol Spectr 10:e0212421.
890 35. Dinarello CA. 2000. Proinflammatory cytokines. Chest 118:503-8.
891 36. Cheng A, Yan H, Han C, Wang W, Tian Y, Chen X. 2014. Polyphenols from blueberries
892 modulate inflammation cytokines in LPS-induced RAW264.7 macrophages. Int J Biol
893 Macromol 69:382-7.
894 37. Liu C, Chu D, Kalantar-Zadeh K, George J, Young HA, Liu G. 2021. Cytokines: From Clinical
895 Significance to Quantification. Adv Sci (Weinh) 8:e2004433.
896 38. Cross AS, Sadoff JC, Kelly N, Bernton E, Gemski P. 1989. Pretreatment with recombinant
897 murine tumor necrosis factor alpha/cachectin and murine interleukin 1 alpha protects mice
898 from lethal bacterial infection. J Exp Med 169:2021-7.
899 39. Huang FC. 2009. Upregulation of Salmonella-induced IL-6 production in Caco-2 cells by PJ-34,
900 PARP-1 inhibitor: involvement of PI3K, p38 MAPK, ERK, JNK, and NF-kappaB. Mediators
901 Inflamm 2009:103890.
902 40. Karki R, Sharma BR, Tuladhar S, Williams EP, Zalduondo L, Samir P, Zheng M, Sundaram B,
903 Banoth B, Malireddi RKS, Schreiner P, Neale G, Vogel P, Webby R, Jonsson CB, Kanneganti TD.
904 2021. Synergism of TNF-alpha and IFN-gamma Triggers Inflammatory Cell Death, Tissue
905 Damage, and Mortality in SARS-CoV-2 Infection and Cytokine Shock Syndromes. Cell 184:149-
906 168 e17.
907 41. Kotas ME, Medzhitov R. 2015. Homeostasis, inflammation, and disease susceptibility. Cell
908 160:816-827.
909 42. Ouyang W, Rutz S, Crellin NK, Valdez PA, Hymowitz SG. 2011. Regulation and functions of the
910 IL-10 family of cytokines in inflammation and disease. Annu Rev Immunol 29:71-109.
911 43. Saraiva M, Vieira P, O'Garra A. 2020. Biology and therapeutic potential of interleukin-10. J Exp
912 Med 217.
913 44. Maloy KJ, Powrie F. 2011. Intestinal homeostasis and its breakdown in inflammatory bowel
914 disease. Nature 474:298-306.
915 45. Hayashi A, Sato T, Kamada N, Mikami Y, Matsuoka K, Hisamatsu T, Hibi T, Roers A, Yagita H,
916 Ohteki T, Yoshimura A, Kanai T. 2013. A single strain of Clostridium butyricum induces
917 intestinal IL-10-producing macrophages to suppress acute experimental colitis in mice. Cell
918 Host Microbe 13:711-22.
919 46. Chen L, Wang D, Garmaeva S, Kurilshikov A, Vich Vila A, Gacesa R, Sinha T, Segal E, Weersma

920 RK, Wijmenga C, Zhernakova A, Fu J. 2021. The long-term genetic stability and individual
921 specificity of the human gut microbiome. Cell 184:2302-2315.e12.
922 47. Wang L, Gou X, Ding Y, Liu J, Wang Y, Wang Y, Zhang J, Du L, Peng W, Fan G. 2023. The
923 interplay between herbal medicines and gut microbiota in metabolic diseases. Front
924 Pharmacol 14:1105405.
925 48. Kaur H, Gupta T, Kapila S, Kapila R. 2021. Protective effects of potential probiotic Lactobacillus
926 rhamnosus (MTCC-5897) fermented whey on reinforcement of intestinal epithelial barrier
927 function in a colitis-induced murine model. Food Funct 12:6102-6116.
928 49. Cani PD, Depommier C, Derrien M, Everard A, de Vos WM. 2022. Akkermansia muciniphila:
929 paradigm for next-generation beneficial microorganisms. Nat Rev Gastroenterol Hepatol
930 19:625-637.
931 50. Polk BF, Kasper DL. 1977. Bacteroides fragilis subspecies in clinical isolates. Ann Intern Med
932 86:569-71.
933 51. Pickard JM, Zeng MY, Caruso R, Núñez G. 2017. Gut microbiota: Role in pathogen colonization,
934 immune responses, and inflammatory disease. Immunol Rev 279:70-89.
935 52. Morgan KL. 2013. Infection, illness, and fenugreek seeds: was illness a good enough proxy for
936 infection in the 2011 outbreak of shiga toxin-producing Escherichia coli O104:H4 in France?
937 Clin Infect Dis 56:1055-6.
938 53. Hardt WD, Chen LM, Schuebel KE, Bustelo XR, Galán JE. 1998. S. typhimurium encodes an
939 activator of Rho GTPases that induces membrane ruffling and nuclear responses in host cells.
940 Cell 93:815-26.
941 54. Parker BJ, Wearsch PA, Veloo ACM, Rodriguez-Palacios A. 2020. The Genus Alistipes: Gut
942 Bacteria With Emerging Implications to Inflammation, Cancer, and Mental Health. Front
943 Immunol 11:906.
944 55. Tang Z, Sun H, Chen T, Lin Z, Jiang H, Zhou X, Shi C, Pan H, Chang O, Ren P, Yu J, Li X, Xu J,
945 Huang Y, Yu X. 2017. Oral delivery of Bacillus subtilis spores expressing cysteine protease of
946 Clonorchis sinensis to grass carp (Ctenopharyngodon idellus): Induces immune responses and
947 has no damage on liver and intestine function. Fish Shellfish Immunol 64:287-296.
948 56. Stothard P, Wishart DS. 2005. Circular genome visualization and exploration using CGView.
949 Bioinformatics 21:537-9.
950 57. Meier-Kolthoff JP, Carbasse JS, Peinado-Olarte RL, Goker M. 2022. TYGS and LPSN: a database
951 tandem for fast and reliable genome-based classification and nomenclature of prokaryotes.
952 Nucleic Acids Res 50:D801-D807.
953 58. Richter M, Rossello-Mora R, Oliver Glockner F, Peplies J. 2016. JSpeciesWS: a web server for
954 prokaryotic species circumscription based on pairwise genome comparison. Bioinformatics
955 32:929-31.
956 59. Chen C, Chen H, Zhang Y, Thomas HR, Frank MH, He Y, Xia R. 2020. TBtools: An Integrative
957 Toolkit Developed for Interactive Analyses of Big Biological Data. Mol Plant 13:1194-1202.
958 60. CLSI. 2018. Performance standards for antimicrobial disk susceptibility tests, M02, 13th ed.
959 Clinical and Laboratory Standards Institute, Wayne, PA.
960 61. Stecher B, Macpherson AJ, Hapfelmeier S, Kremer M, Stallmach T, Hardt WD. 2005.
961 Comparison of Salmonella enterica serovar Typhimurium colitis in germfree mice and mice
962 pretreated with streptomycin. Infect Immun 73:3228-41.
963 62. Praveschotinunt P, Duraj-Thatte AM, Gelfat I, Bahl F, Chou DB, Joshi NS. 2019. Engineered E.

964 coli Nissle 1917 for the delivery of matrix-tethered therapeutic domains to the gut. Nat
965 Commun 10:5580.

966

967 **Figure legends**

968

969 **Fig. 1 Genomic characteristics and phylogenetic relationships of *B.***
970 ***velezensis* HBXN2020.** (**A**) The whole-genome map of *B. velezensis*
971 HBXN2020 with its genomic features. The map consists of 6 circles. From the
972 inner circle to the outer circle: (1) GC-skew, (2) GC content, (3) reverse
973 protein-coding genes, different colors represents different COG functional
974 classifications, (4) genes transcribed in reverse direction, (5) genes
975 transcribed in forward direction, (6) forward protein-coding genes, different
976 colors represents different COG functional classifications. (**B**) The whole
977 genome phylogenetic tree was constructed based on genome-wide data from
978 14 bacillus strains. *B. velezensis* HBXN2020 are indicated in bold. (**C**) The
979 heatmap based on the ANIb value of strain HBXN2020 and other Bacillus
980 species. The *B. velezensis* HBXN2020 was labeled in red letters.

981

982 **Fig. 2 Growth curve of *B. velezensis* HBXN2020 and its *in vitro***
983 **resistance against environmental assaults.** (**A**) Growth curves of *B.*
984 *velezensis* HBXN2020 cultured in LB medium at 37°C, detection of OD_{600}
985 values at 1 h intervals in microplate reader. (**B**) Survival rate of endospore
986 and vegetative cells of *B. velezensis* HBXN2020 after 30 min at different

987 temperatures (37°C, 45°C, 55°C, 65°C, 75°C, 85°C or 95°C). Equal amounts
988 of endospore and vegetative cells of HBXN2020 were exposed to the
989 following: (**C**) acid solution (pH 2 to 7), (**D**) 0.3% bile salts, (**E**) SGF (pH 1.2)
990 supplemented with pepsin, and (**F**) SIF (pH 6.8) containing trypsin at 37°C. At
991 predetermined time points, 100 μL was taken from each sample, and tenfold
992 serially diluted with sterile PBS (pH 7.2), and then spread on LB agar plates
993 and cultured at 37°C for 12 h before bacterial counting. Each group was
994 repeated three times (n = 3).
995
996 **Fig. 3 Antibiotic susceptibility of *B. velezensis* HBXN2020 and**
997 **bacteriostasis assay *in vitro*.** (**A**) The diameter of the antibacterial zone
998 indicates the extent of sensitivity to antibiotics. (**B**) The diameter of the
999 antibacterial zone indicates the extent of inhibition against pathogenic bacteria.
1000 The diameter of the antibacterial zone was measured with vernier caliper.
1001 Each group was repeated three times (n = 3). R, resistant; I, moderately
1002 sensitive; S, sensitive.
1003
1004 **Fig. 4 *In vivo* safety evaluation of *B. velezensis* HBXN2020 in a mouse**
1005 **model.** (**A**) Body weights changes of mice during gavage with *B. velezensis*
1006 HBXN2020 spores. Mice were treated with sterile PBS (Control group) or low-
1007 dose (L-HBXN2020 group), medium dose (M-HBXN2020 group), and high-
1008 dose (H-HBXN2020 group) of *B. velezensis* HBXN2020 spores. Weighing and

1009 gavage were performed once every two days during the experimental period
1010 (15 days). Data were shown as mean values ± SEM (n = 5). (**B**) The relative
1011 gene expression levels of inflammatory cytokines in the colon of mice
1012 measured by RT-qPCR. Data were shown as mean values ± SEM (n = 5). (**C**)
1013 The relative gene expression levels of barrier protein ZO-1, occludin, claudin
1014 and Muc2 in the colon of mice measured by RT-qPCR. Data were shown as
1015 mean values ± SEM (n = 5). (**D**) Major blood routine parameters and (**E**)
1016 serum biochemical parameters of mice in the control group and H-HBXN2020
1017 group. Data were shown as mean values ± SEM (n = 3). (**F**) H&E stained
1018 colon sections in the different groups. Scale bar: 200 μm.
1019
1020 **Fig. 5 Oral *B. velezensis* HBXN2020 spores alleviated *S.* Typhimurium-**
1021 **induced experimental mouse colitis.** (**A**) *In vitro* Bacterial competition
1022 between STm and *B. velezensis* HBXN2020. STm were co-incubated with *B.*
1023 *velezensis* HBXN2020 at various ratios at 37°C with shaking. The growth of
1024 STm was reflected by bacterial counting per hour. (**B**) Experimental design for
1025 treatment in this study. Orally administrated with either PBS, or *B. velezensis*
1026 HBXN2020 spores by gavage at days 1, 3, and 5 after STm infection (5×10^7
1027 CFU/mouse), respectively. All mice were euthanized at day 7 after STm
1028 infection. (**C**) Bacterial count of STm in mouse feces. Fecal samples were
1029 collected per day after STm infection and resuspended in sterile PBS (0.1 g of
1030 fecal resuspended in 1 mL of sterile PBS). One hundred microliters of each

1031 sample performed a serial of 10-fold dilutions and spread on selective agar
1032 plates (50 μg mL^{-1} kanamycin) and incubated at 37°C for 12 h before bacterial
1033 counting. The bacterial loads of STm in (**D**) cecum, and (**E**) colon. The cecum
1034 and colon were harvested and then homogenized. One hundred microliters of
1035 each sample performed a serial of 10-fold dilutions and spread on selective
1036 agar plates (50 μg mL^{-1} kanamycin) and incubated at 37°C for 12 h before
1037 bacterial counting. Statistical signifcance was evaluated using Student's t-test
1038 (*, $P < 0.05$, **, $P < 0.01$, and ***, $P < 0.001$). (**F**) Daily body weight changes
1039 and (**G**) daily disease activity index (DAI) scores of mice with different
1040 treatment groups. Data were shown as mean values ± SEM (n = 8). Statistical
1041 signifcance was evaluated using one-way analysis of variance (ANOVA) with
1042 Tukey's multiple comparisons test. *, $P < 0.05$, **, $P < 0.01$, and ***, $P < 0.001$
1043 relative to Control group; $^{\#}$, $P < 0.05$, $^{\#\#}$, $P < 0.01$, $^{\#\#\#}$, $P < 0.001$ relative to
1044 STm + HBXN2020 group. (**H**) Colonic tissue images. (**I**) The length of the
1045 colon from per group (n = 8). Statistical signifcance was evaluated using one-
1046 way analysis of variance (ANOVA) with Tukey's multiple comparisons test (*,
1047 $P < 0.05$, **, $P < 0.01$, and ***, $P < 0.001$).
1048
1049 **Fig. 6 Oral *B. velezensis* HBXN2020 spores attenuated colonic damage**
1050 **and inflammatory reaction.** (**A**) H&E stained colon tissue sections. Scale bar:
1051 200 μm. The relative gene expression levels of TNF-α (**B**), IL-1β (**C**), IL-6 (**D**),
1052 and IL-10 (**E**) were detected by RT-qPCR. Data were shown as mean values

± SEM (n = 6). The relative gene expression levels of ZO-1 (**F**), ocludin (**G**), claudin (**H**), and Muc2 (**I**) in colon tissue were detected by RT-qPCR. Data were shown as mean values ± SEM (n = 6). Statistical signifcance was evaluated using one-way analysis of variance (ANOVA) with Tukey's multiple comparisons test (*, $P < 0.05$, **, $P < 0.01$, and ***, $P < 0.001$).

Fig. 7 Oral *B. velezensis* HBXN2020 spores regulated the composition of intestinal microbiota. (**A** to **D**) The α-diversity of the gut microbiota, determined by the (**A**) Sobs, (**B**) Chao1, (**C**) Shannon, and (**D**) Simpson diversity index. Data were shown as mean values ± SEM (n = 5). (**E**) The PCA plot showed the β-diversity of the gut microbiota based on Bray-Curtis distance at the OTU level. (**F** and **G**) The relative abundance of colonic microbiota at the phylum (**F**) and genus (**G**) levels. (**H-K**) Relative abundance of selected taxa (**H**) *norank_f_Muribaculaceae*, (**I**) *Lactobacillus*, (**J**) *Bacteroides*, and (**K**) *Escherichia-Shigella*. Data were shown as mean values ± SEM (n = 5). (**L**) Analysis of differences in the microbial communities by LEfSe (linear discriminant analysis (LDA) score > 3.5) among different groups. Signifcance was evaluated by the Kruskal-Wallis test or ANOVA with Tukey's multiple comparisons test (*, P < 0.05, **, P < 0.01, and ***, P < 0.001).

Fig. 8 Prophylactic *B. velezensis* HBXN2020 spores attenuated the symptoms of *S.* Typhimurium-induced mouse colitis. (**A**) Experimental

1075 design for treatment in this study. At days 1, 3, 5, and 7, each mouse in the
1076 HBXN2020 + STm group and PBS + STm group were received 200 μL (1×10^8
1077 CFU/mouse) of *B. velezensis* HBXN2020 spores or sterile PBS by gavage.
1078 Then, mice in PBS + STm group and HBXN2020 + STm group were orally
1079 inoculated with 200 μL (5×10^7 CFU/mouse) of STm on day 7. On day 12, all
1080 mice were euthanized. (**B**) Daily body weight changes and (**C**) daily disease
1081 activity index (DAI) scores of mice with different groups following STm
1082 treatment. Data were shown as mean values ± SEM (n = 8). Statistical
1083 signifcance was evaluated using one-way analysis of variance (ANOVA) with
1084 Tukey's multiple comparisons test. *, $P < 0.05$, **, $P < 0.01$, and ***, $P < 0.001$
1085 relative to Control group; $^{\#}$, $P < 0.05$, $^{\#\#}$, $P < 0.01$, $^{\#\#\#}$, $P < 0.001$ relative to
1086 HBXN2020 + STm group. (**D**) Colonic tissue images. (**E**) The length of the
1087 colon from per group (n = 8). (**F**) Bacterial count of STm in mouse feces.
1088 Fecal samples were collected every day after STm infection and resuspended
1089 in sterile PBS (0.1 g of fecal resuspended in 1 mL of sterile PBS). One
1090 hundred microliters of each sample performed a serial of 10-fold dilutions and
1091 spread on selective agar plates (50 μg mL^{-1} kanamycin) and incubated at
1092 37°C for 12 h before bacterial counting. The bacterial loads of STm in
1093 (**G**)cecum and (**H**)colon. The cecum and colon were harvested and then
1094 homogenized. One hundred microliters of each sample performed a serial of
1095 10-fold dilutions and spread on selective agar plates (50 μg mL^{-1} kanamycin)
1096 and incubated at 37°C for 12 h before bacterial counting. Statistical

1097 signifcance was evaluated using Student's t-test (*, $P < 0.05$, **, $P < 0.01$, and
1098 ***, $P < 0.001$).
1099
1100 **Fig. 9 Prophylactic *B. velezensis* HBXN2020 spores attenuated colonic**
1101 **damage and inflammatory reaction.** (**A**) H&E stained colon tissue sections.
1102 Scale bar: 200 μm. The relative gene expression levels of TNF-α (**B**), IL-1β
1103 (**C**), IL-6 (**D**), and IL-10 (**E**) were detected by RT-qPCR. Data were shown as
1104 mean values ± SEM (n = 6). The relative gene expression levels of ZO-1 (**F**),
1105 ocludin (**G**), claudin (**H**), and Muc2 (**I**) in colon tissue were detected by RT-
1106 qPCR. Data were shown as mean values ± SEM (n = 6). Statistical
1107 signifcance was evaluated using one-way analysis of variance (ANOVA) with
1108 Tukey's multiple comparisons test (*, $P < 0.05$, **, $P < 0.01$, and ***, $P < 0.001$).
1109
1110 **Fig. 10 Prophylactic *B. velezensis* HBXN2020 spores regulated the**
1111 **composition of gut microbiota.** (**A** to **D**) Alpha diversity of the intestinal
1112 microbiota. Data were shown as mean values ± SEM (n = 5). (**E**) The PCA
1113 plot showed the β-diversity among different microbial community groups
1114 based on Bray-Curtis distance at the OTU level. (**F** and **G**) The relative
1115 abundance of colonic microbiota at the phylum (**F**) and genus (**G**) levels. (**H-M**)
1116 Relative abundance of selected taxa (**H**) *Lactobacillus*, (**I**) *Akkermansia*, (**J**)
1117 *Alistipes*, (**K**) *Bacteroides*, (**L**) *Escherichia-Shigella*, and (**M**) *Enterococcus*.
1118 Data were shown as mean values ± SEM (n = 5). (**N**) Analysis of differences

1119 in the microbial taxa by LEfSe (LDA score > 3.5) in different groups.
1120 Signifcance was evaluated by the Kruskal-Wallis test or ANOVA with Tukey's
1121 multiple comparisons test (*, $P < 0.05$, **, $P < 0.01$, and ***, $P < 0.001$).
1122

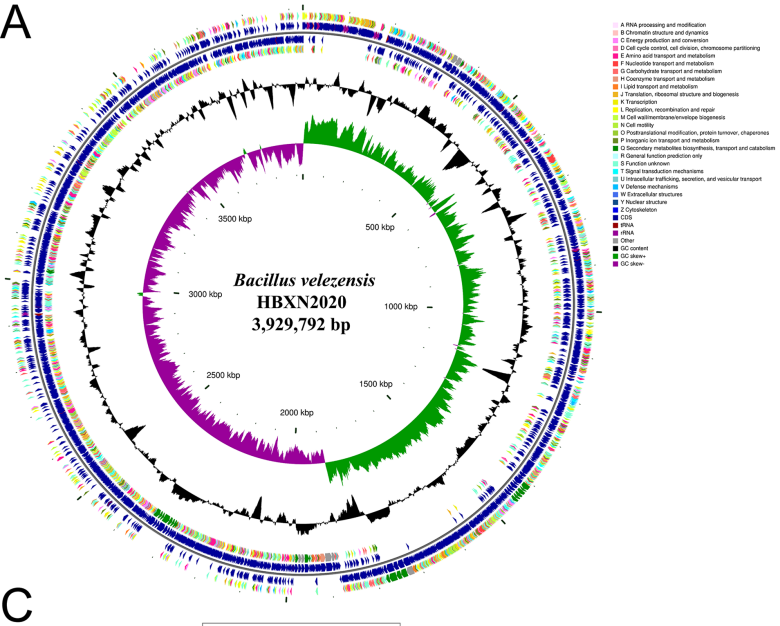
A
Bacillus velezensis
HBXN2020
3,929,792 bp
500 kbp
1000 kbp
1500 kbp
2000 kbp
2500 kbp
3000 kbp
3500 kbp
A RNA processing and modification
B Chromatin structure and dynamics
C Energy production and conversion
D Cell cycle control, cell division, chromosome partitioning
E Amino acid transport and metabolism
F Nucleotide transport and metabolism
G Carbohydrate transport and metabolism
H Coenzyme transport and metabolism
I Lipid transport and metabolism
J Translation, ribosomal structure and biogenesis
K Transcription
L Replication, recombination and repair
M Cell wall/membrane/envelope biogenesis
N Cell motility
O Posttranslational modification, protein turnover, chaperones
P Inorganic ion transport and metabolism
Q Secondary metabolites biosynthesis, transport and catabolism
R General function prediction only
S Function unknown
T Signal transduction mechanisms
U Intracellular trafficking, secretion, and vesicular transport
V Defense mechanisms
W Extracellular structures
Y Nuclear structure
Z Cytoskeleton
CDS
tRNA
rRNA
Other
GC content
GC skew+
GC skew-

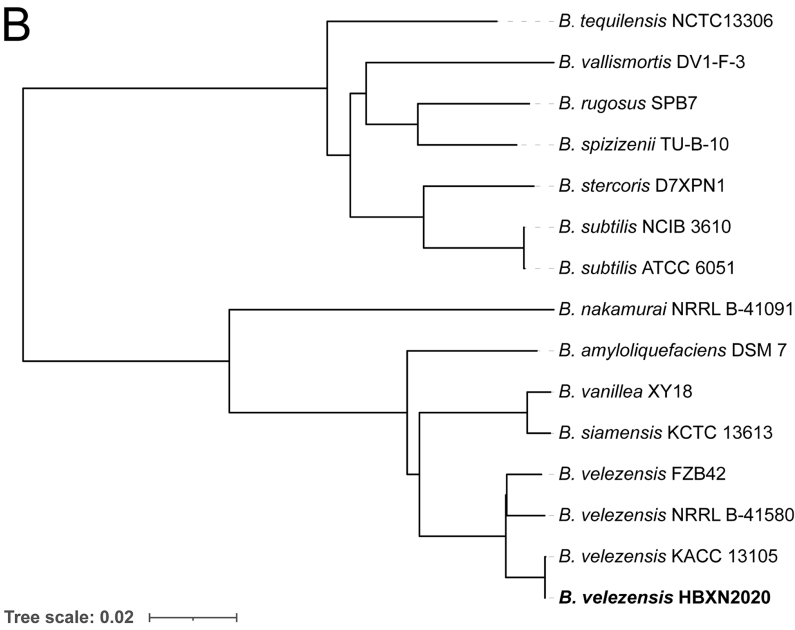
B
B. tequilensis NCTC13306
B. vallismortis DV1-F-3
B. rugosus SPB7
B. spizizenii TU-B-10
B. stercoris D7XPN1
B. subtilis NCIB 3610
B. subtilis ATCC 6051
B. nakamurai NRRL B-41091
B. amyloliquefaciens DSM 7
B. vanillea XY18
B. siamensis KCTC 13613
B. velezensis FZB42
B. velezensis NRRL B-41580
B. velezensis KACC 13105
B. velezensis HBXN2020
Tree scale: 0.02

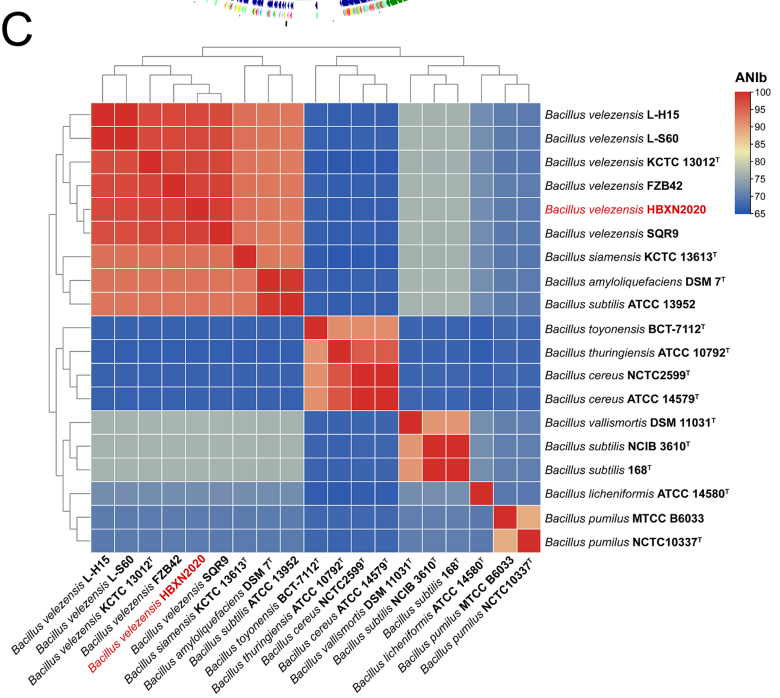
C
ANIb
100
95
90
85
80
75
70
65
Bacillus velezensis L-H15
Bacillus velezensis L-S60
Bacillus velezensis KCTC 13012T
Bacillus velezensis FZB42
Bacillus velezensis HBXN2020
Bacillus velezensis SQR9
Bacillus siamensis KCTC 13613T
Bacillus amyloliquefaciens DSM 7T
Bacillus subtilis ATCC 13952
Bacillus toyonensis BCT-7112T
Bacillus thuringiensis ATCC 10792T
Bacillus cereus NCTC2599T
Bacillus cereus ATCC 14579T
Bacillus vallismortis DSM 11031T
Bacillus subtilis NCIB 3610T
Bacillus subtilis 168T
Bacillus licheniformis ATCC 14580T
Bacillus pumilus MTCC B6033
Bacillus pumilus NCTC10337T

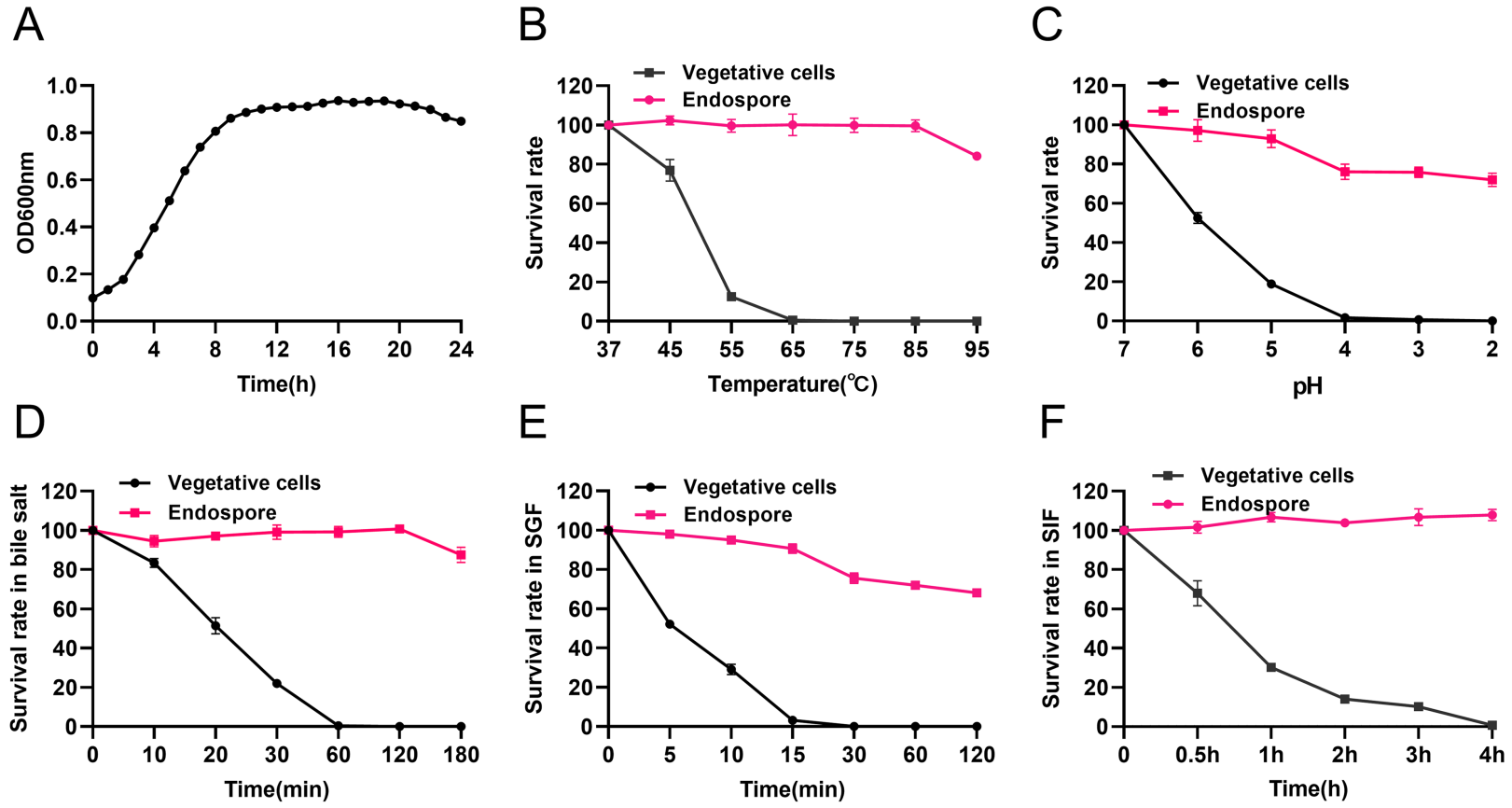
A
OD600nm
Time(h)
B
Vegetative cells
Endospore
Survival rate
Temperature(℃)
C
Vegetative cells
Endospore
Survival rate
pH
D
Vegetative cells
Endospore
Survival rate in bile salt
Time(min)
E
Vegetative cells
Endospore
Survival rate in SGF
Time(min)
F
Vegetative cells
Endospore
Survival rate in SIF
Time(h)

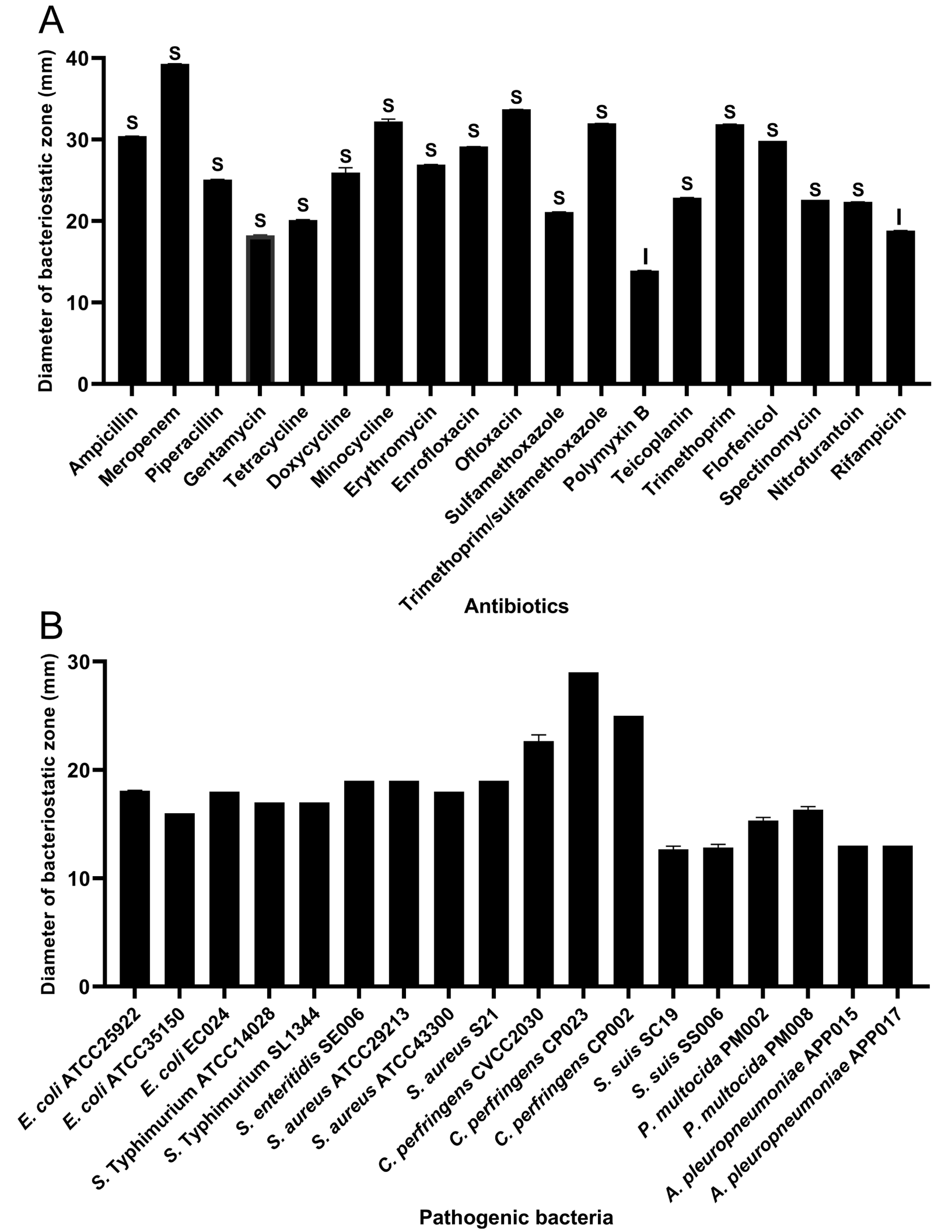
A
Diameter of bacteriostatic zone (mm)
0
10
20
30
40
S
S
S
S
S
S
S
S
S
S
S
S
I
S
S
S
S
I
Ampicillin
Meropenem
Piperacillin
Gentamycin
Tetracycline
Doxycycline
Minocycline
Erythromycin
Enrofloxacin
Ofloxacin
Sulfamethoxazole
Trimethoprim/sulfamethoxazole
Polymyxin B
Teicoplanin
Trimethoprim
Florfenicol
Spectinomycin
Nitrofurantoin
Rifampicin
Antibiotics
B
Diameter of bacteriostatic zone (mm)
0
10
20
30
E. coli ATCC25922
E. coli ATCC35150
E. coli EC024
S. Typhimurium ATCC14028
S. Typhimurium SL1344
S. enteritidis SE006
S. aureus ATCC29213
S. aureus ATCC43300
S. aureus S21
C. perfringens CVCC2030
C. perfringens CP023
C. perfringens CP002
S. suis SC19
S. suis SS006
P. multocida PM002
P. multocida PM008
A. pleuropneumoniae APP015
A. pleuropneumoniae APP017
Pathogenic bacteria

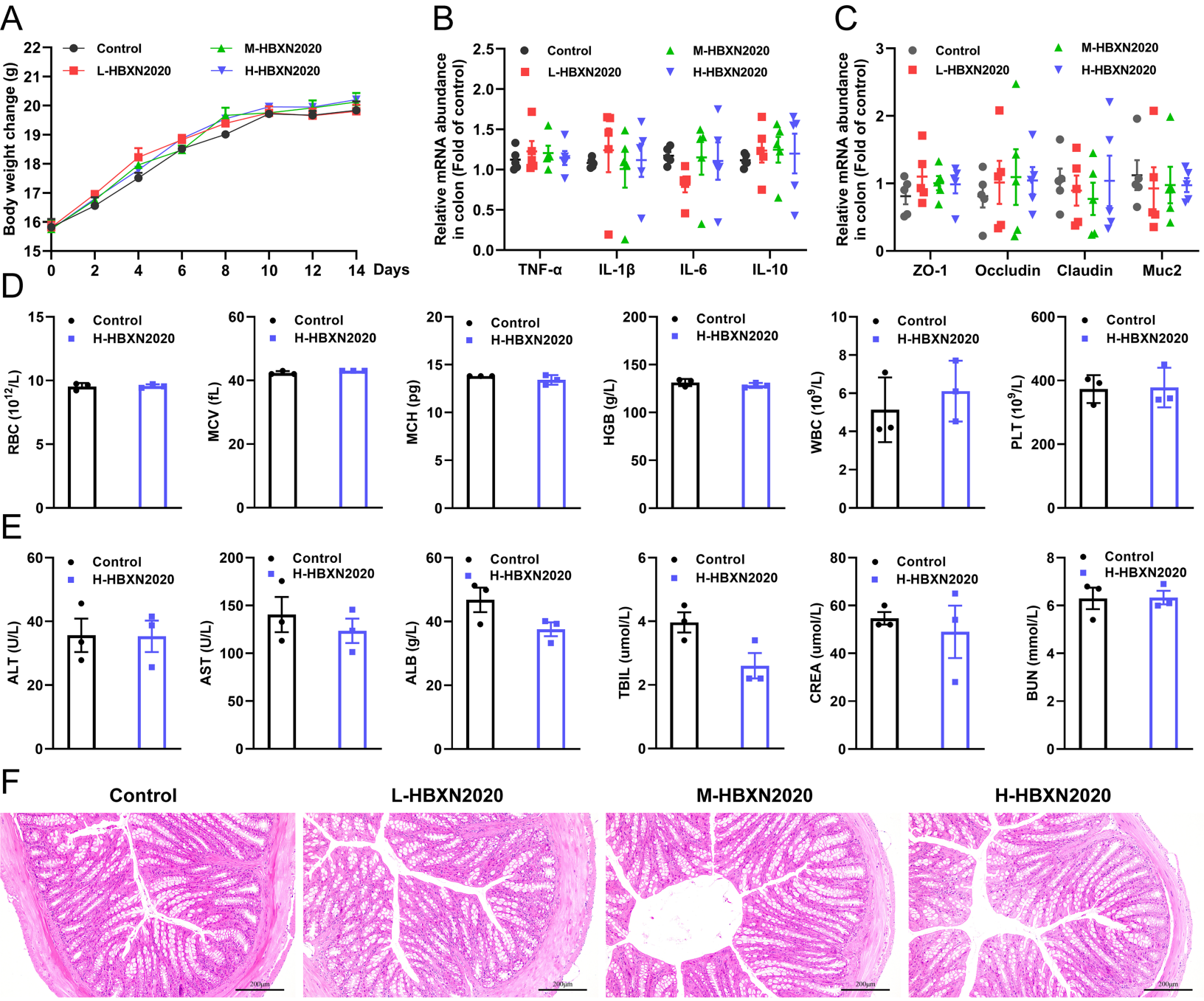
A
Control
L-HBXN2020
M-HBXN2020
H-HBXN2020
Body weight change (g)
Days
B
Relative mRNA abundance in colon (Fold of control)
TNF-α
IL-1β
IL-6
IL-10
C
ZO-1
Occludin
Claudin
Muc2
D
RBC (10^{12}/L)
MCV (fL)
MCH (pg)
HGB (g/L)
WBC (10^9/L)
PLT (10^9/L)
E
ALT (U/L)
AST (U/L)
ALB (g/L)
TBIL (umol/L)
CREA (umol/L)
BUN (mmol/L)
F
Control
L-HBXN2020
M-HBXN2020
H-HBXN2020

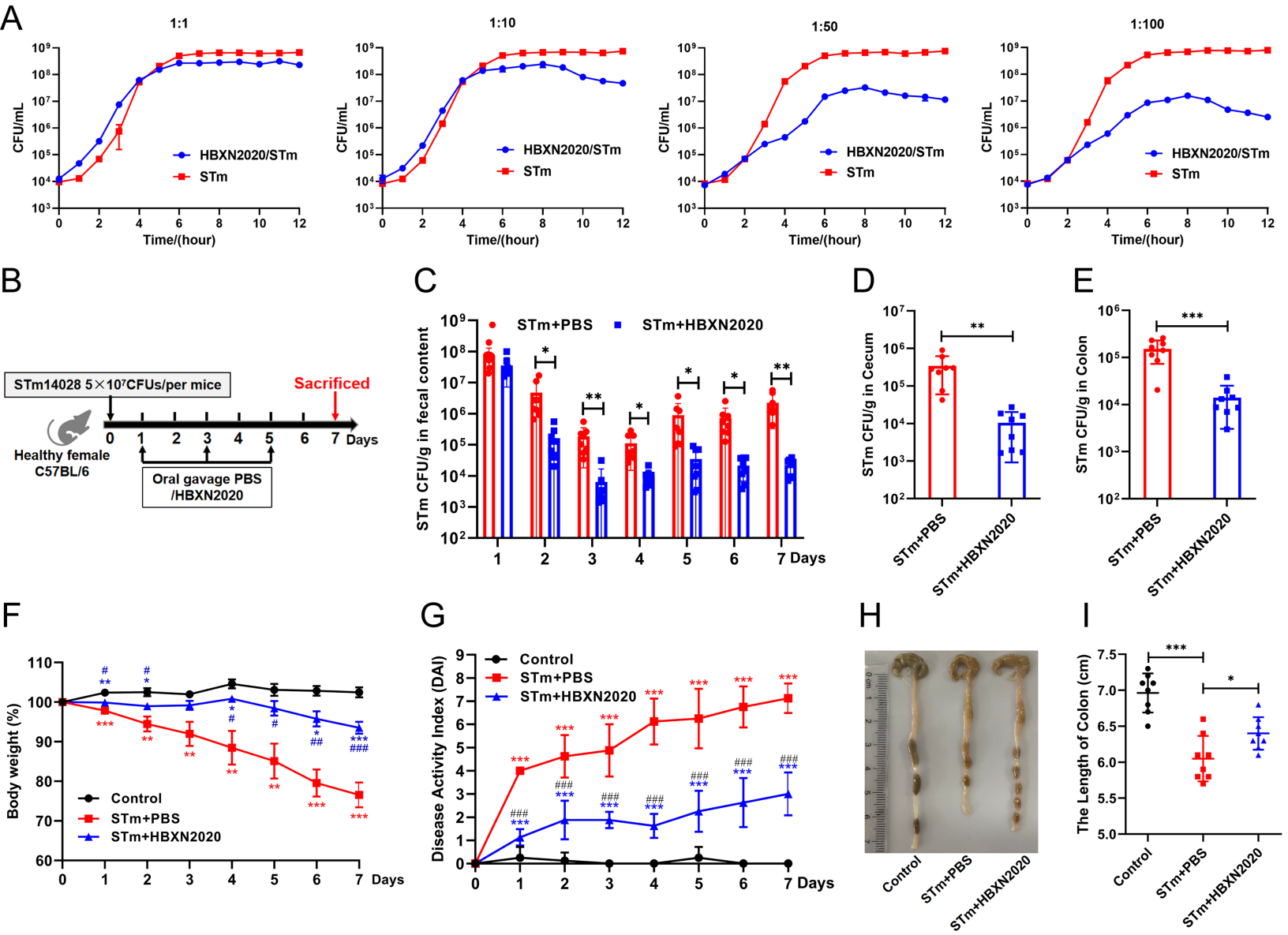
A
1:1
1:10
1:50
1:100
CFU/mL
Time/(hour)
HBXN2020/STm
STm
B
STm14028 5×10⁷CFUs/per mice
Sacrificed
Healthy female C57BL/6
Oral gavage PBS /HBXN2020
Days
C
STm+PBS
STm+HBXN2020
STm CFU/g in fecal content
Days
D
STm CFU/g in Cecum
E
STm CFU/g in Colon
F
Body weight (%)
Control
STm+PBS
STm+HBXN2020
Days
G
Disease Activity Index (DAI)
Control
STm+PBS
STm+HBXN2020
Days
H
Control
STm+PBS
STm+HBXN2020
I
The Length of Colon (cm)
Control
STm+PBS
STm+HBXN2020

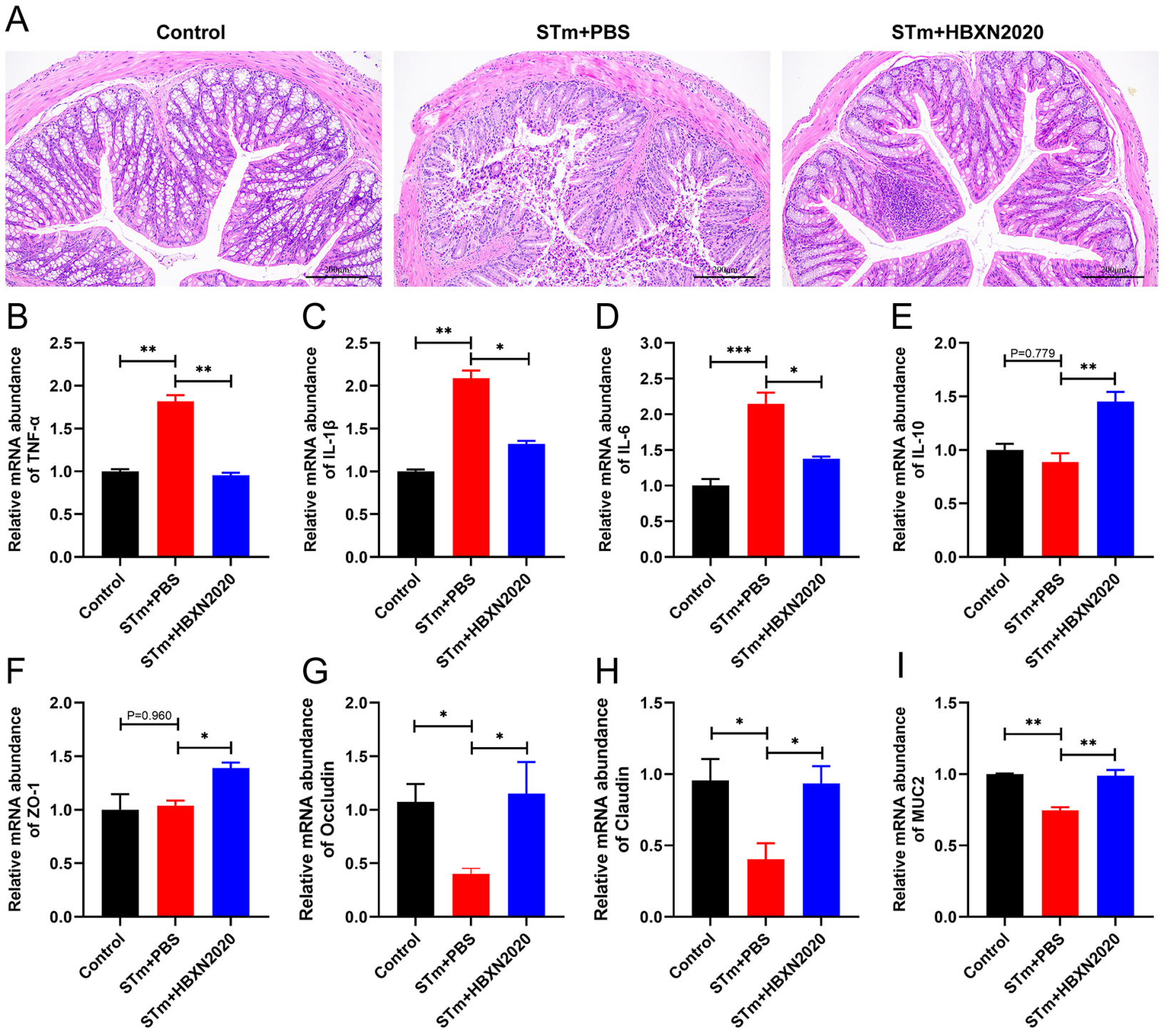
A
Control
STm+PBS
STm+HBXN2020
200μm
B
Relative mRNA abundance of TNF-α
C
Relative mRNA abundance of IL-1β
D
Relative mRNA abundance of IL-6
E
Relative mRNA abundance of IL-10
P=0.779
F
Relative mRNA abundance of ZO-1
P=0.960
G
Relative mRNA abundance of Occludin
H
Relative mRNA abundance of Claudin
I
Relative mRNA abundance of MUC2
Control
STm+PBS
STm+HBXN2020

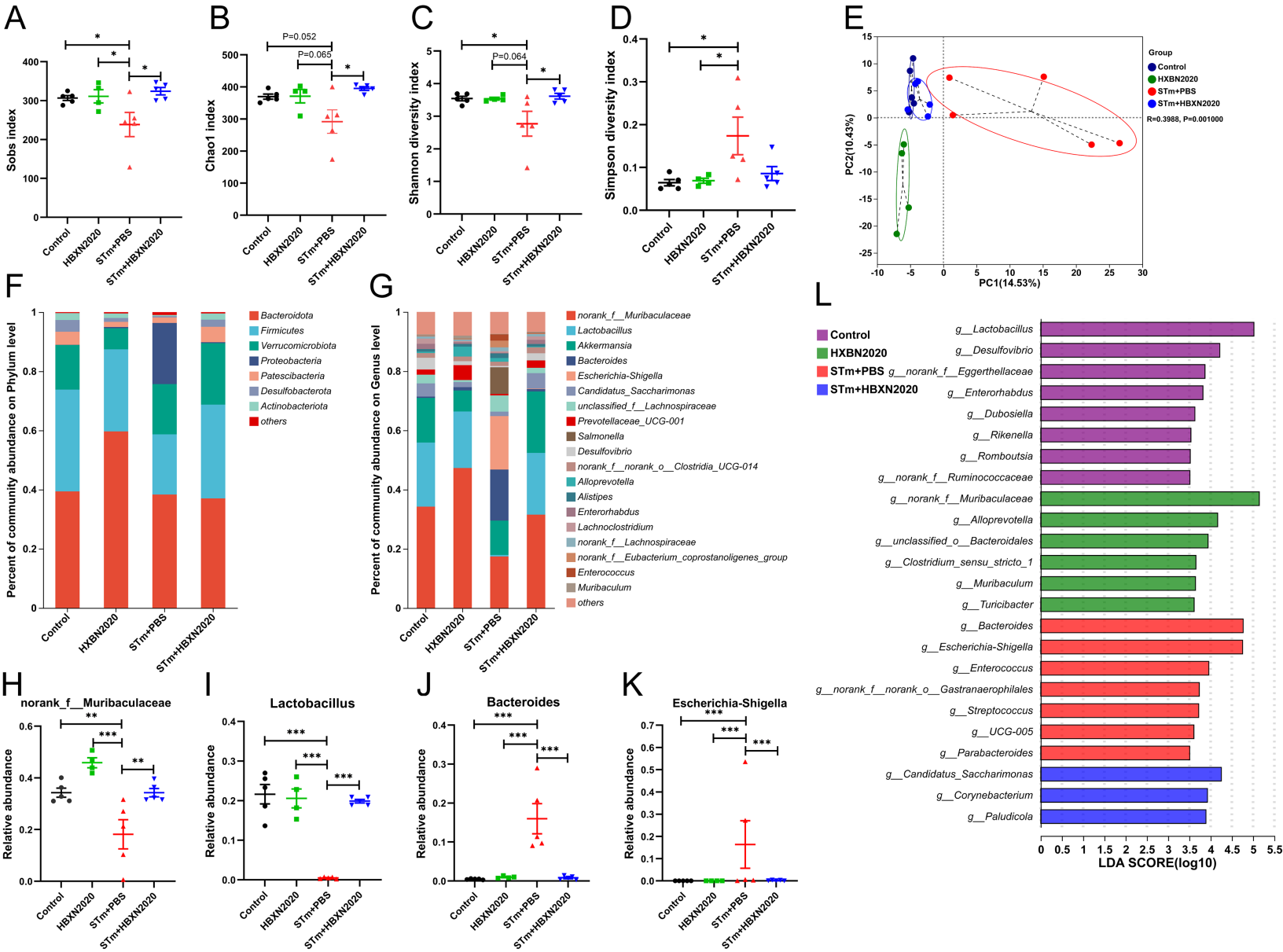
A
Sobs index
Control
HBXN2020
STm+PBS
STm+HBXN2020
B
Chao1 index
P=0.052
P=0.065
C
Shannon diversity index
P=0.064
D
Simpson diversity index
E
Group
Control
HXBN2020
STm+PBS
STm+HBXN2020
R=0.3988, P=0.001000
PC1(14.53%)
PC2(10.43%)
F
Percent of community abundance on Phylum level
Bacteroidota
Firmicutes
Verrucomicrobiota
Proteobacteria
Patescibacteria
Desulfobacterota
Actinobacteriota
others
G
Percent of community abundance on Genus level
norank_f__Muribaculaceae
Lactobacillus
Akkermansia
Bacteroides
Escherichia-Shigella
Candidatus_Saccharimonas
unclassified_f__Lachnospiraceae
Prevotellaceae_UCG-001
Salmonella
Desulfovibrio
norank_f__norank_o__Clostridia_UCG-014
Alloprevotella
Alistipes
Enterorhabdus
Lachnoclostridium
norank_f__Lachnospiraceae
norank_f__Eubacterium_coprostanoligenes_group
Enterococcus
Muribaculum
others
H
norank_f__Muribaculaceae
Relative abundance
I
Lactobacillus
J
Bacteroides
K
Escherichia-Shigella
L
Control
HXBN2020
STm+PBS
STm+HBXN2020
g__Lactobacillus
g__Desulfovibrio
g__norank_f__Eggerthellaceae
g__Enterorhabdus
g__Dubosiella
g__Rikenella
g__Romboutsia
g__norank_f__Ruminococcaceae
g__norank_f__Muribaculaceae
g__Alloprevotella
g__unclassified_o__Bacteroidales
g__Clostridium_sensu_stricto_1
g__Muribaculum
g__Turicibacter
g__Bacteroides
g__Escherichia-Shigella
g__Enterococcus
g__norank_f__norank_o__Gastranaerophilales
g__Streptococcus
g__UCG-005
g__Parabacteroides
g__Candidatus_Saccharimonas
g__Corynebacterium
g__Paludicola
LDA SCORE(log10)

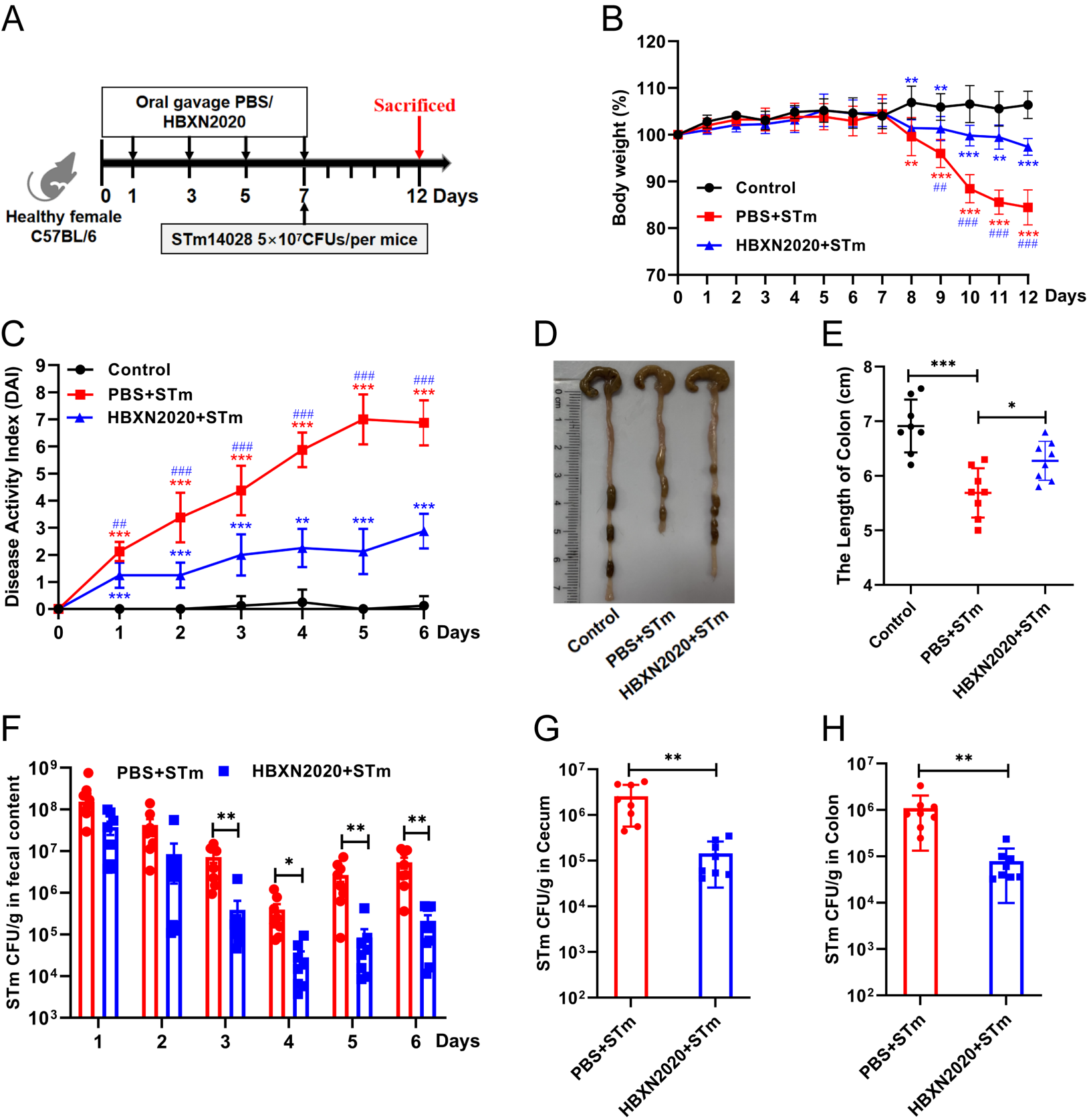
A
Oral gavage PBS/ HBXN2020
Sacrificed
Healthy female C57BL/6
0 1 3 5 7 12 Days
STm14028 5×10⁷CFUs/per mice
B
Body weight (%)
Control
PBS+STm
HBXN2020+STm
Days
C
Disease Activity Index (DAI)
Control
PBS+STm
HBXN2020+STm
Days
D
Control
PBS+STm
HBXN2020+STm
E
The Length of Colon (cm)
Control
PBS+STm
HBXN2020+STm
F
STm CFU/g in fecal content
PBS+STm
HBXN2020+STm
Days
G
STm CFU/g in Cecum
PBS+STm
HBXN2020+STm
H
STm CFU/g in Colon
PBS+STm
HBXN2020+STm

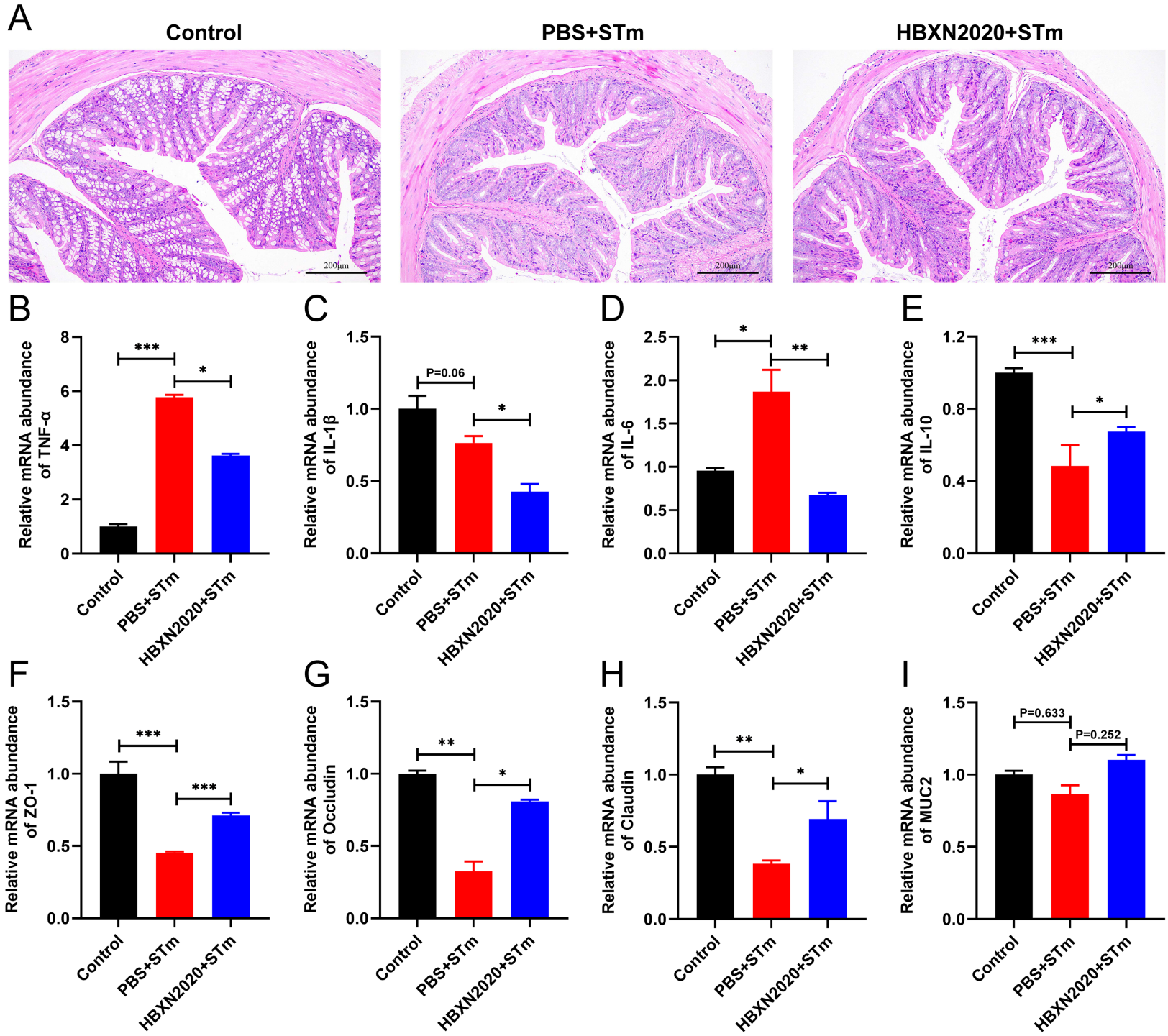
A
Control
PBS+STm
HBXN2020+STm
200μm
B
Relative mRNA abundance of TNF-α
C
Relative mRNA abundance of IL-1β
P=0.06
D
Relative mRNA abundance of IL-6
E
Relative mRNA abundance of IL-10
F
Relative mRNA abundance of ZO-1
G
Relative mRNA abundance of Occludin
H
Relative mRNA abundance of Claudin
I
Relative mRNA abundance of MUC2
P=0.633
P=0.252
Control
PBS+STm
HBXN2020+STm

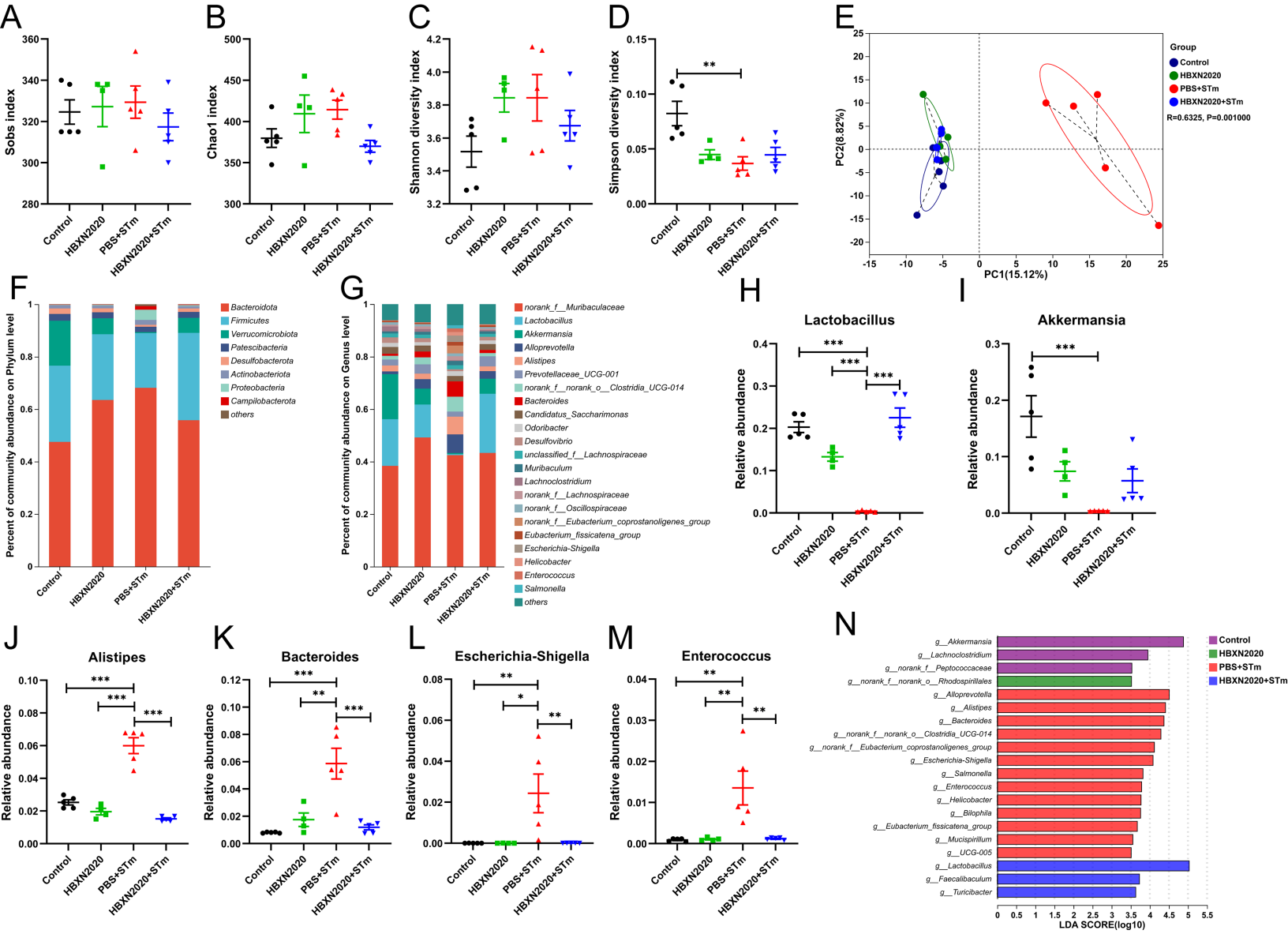
A
Sobs index
B
Chao1 index
C
Shannon diversity index
D
Simpson diversity index
Control
HBXN2020
PBS+STm
HBXN2020+STm
E
Group
Control
HBXN2020
PBS+STm
HBXN2020+STm
R=0.6325, P=0.001000
PC1(15.12%)
PC2(8.82%)
F
Percent of community abundance on Phylum level
Bacteroidota
Firmicutes
Verrucomicrobiota
Patescibacteria
Desulfobacterota
Actinobacteriota
Proteobacteria
Campilobacterota
others
G
Percent of community abundance on Genus level
norank_f__Muribaculaceae
Lactobacillus
Akkermansia
Alloprevotella
Alistipes
Prevotellaceae_UCG-001
norank_f__norank_o__Clostridia_UCG-014
Bacteroides
Candidatus_Saccharimonas
Odoribacter
Desulfovibrio
unclassified_f__Lachnospiraceae
Muribaculum
Lachnoclostridium
norank_f__Lachnospiraceae
norank_f__Oscillospiraceae
norank_f__Eubacterium_coprostanoligenes_group
Eubacterium_fissicatena_group
Escherichia-Shigella
Helicobacter
Enterococcus
Salmonella
others
H
Lactobacillus
Relative abundance
I
Akkermansia
J
Alistipes
K
Bacteroides
L
Escherichia-Shigella
M
Enterococcus
N
g__Akkermansia
g__Lachnoclostridium
g__norank_f__Peptococcaceae
g__norank_f__norank_o__Rhodospirillales
g__Alloprevotella
g__Alistipes
g__Bacteroides
g__norank_f__norank_o__Clostridia_UCG-014
g__norank_f__Eubacterium_coprostanoligenes_group
g__Escherichia-Shigella
g__Salmonella
g__Enterococcus
g__Helicobacter
g__Bilophila
g__Eubacterium_fissicatena_group
g__Mucispirillum
g__UCG-005
g__Lactobacillus
g__Faecalibaculum
g__Turicibacter
LDA SCORE(log10)